

The M-dwarfs in Multiples (MINMS) survey – I. Stellar multiplicity among low-mass stars within 15 pc[★]

K. Ward-Duong,^{1†} J. Patience,¹ R. J. De Rosa,^{1,2,3} J. Bulger,¹ A. Rajan,¹
S. P. Goodwin,⁴ Richard J. Parker,⁵ D. W. McCarthy⁶ and C. Kulesa⁶

¹School of Earth and Space Exploration, Arizona State University, Tempe, AZ 85287, USA

²Astrophysics Group, School of Physics, University of Exeter, Stocker Road, Exeter EX4 4QL, UK

³Department of Astronomy, University of California, Berkeley, CA 94720, USA

⁴Department of Physics and Astronomy, University of Sheffield, Hounsfield Road, Sheffield S3 7RH, UK

⁵Astrophysics Research Institute, Liverpool John Moores University, 146 Brownlow Hill, Liverpool L3 5RF, UK

⁶Steward Observatory, University of Arizona, 933 N. Cherry Ave., Tucson, AZ 85721, USA

Accepted 2015 February 20. Received 2015 February 19; in original form 2014 June 9

ABSTRACT

We present a large-scale, volume-limited companion survey of 245 late-K to mid-M (K7–M6) dwarfs within 15 pc. Infrared adaptive optics (AO) data were analysed from the Very Large Telescope, Subaru Telescope, Canada–France–Hawaii Telescope, and MMT Observatory to detect close companions to the sample from ~ 1 to 100 au, while digitized wide-field archival plates were searched for wide companions from ~ 100 to 10 000 au. With sensitivity to the bottom of the main sequence over a separation range of 3 to 10 000 au, multiple AO and wide-field epochs allow us to confirm candidates with common proper motions, minimize background contamination, and enable a measurement of comprehensive binary statistics. We detected 65 comoving stellar companions and find a companion star fraction of 23.5 ± 3.2 per cent over the 3 au to 10 000 au separation range. The companion separation distribution is observed to rise to a higher frequency at smaller separations, peaking at closer separations than measured for more massive primaries. The mass ratio distribution across the $q = 0.2\text{--}1.0$ range is flat, similar to that of multiple systems with solar-type primaries. The characterization of binary and multiple star frequency for low-mass field stars can provide crucial comparisons with star-forming environments and hold implications for the frequency and evolutionary histories of their associated discs and planets.

Key words: techniques: high angular resolution – binaries: close – binaries: general – binaries: visual – stars: late-type – stars: low-mass.

1 INTRODUCTION

Among the nearest stars, the large majority are M-dwarfs (e.g. Reid & Gizis 1997), with a recent accounting indicating that M-dwarfs outnumber higher mass stars by a factor of ~ 3 (Lépine & Gaidos 2011). Ongoing parallax programme designed to survey the Solar Neighbourhood continue to discover additional nearby M-dwarfs, increasing the proportion of the lowest mass members among the nearest stars (e.g. Henry et al. 2006). The nearest star-

forming regions are also dominated by low-mass stars; for example, ~ 50 per cent of the known members of Taurus have spectral types later than M3, the spectral type that will correspond to M0 and later after contraction on to the main sequence (Luhman et al. 2010). The preponderance of the low-mass population of stars highlights the importance of understanding their properties, including the statistics of their companions. As they represent a common outcome of star formation, multiple star systems provide key signatures of the physical processes which affect both star and planet formation.

One of the key scientific questions of star formation is the universality of the process, and the distribution of binary stars and the initial mass function (IMF) are among the main observational products that can be used to investigate this area (King et al. 2012a). There is no evidence that the IMF varies systematically between different environments (e.g. Luhman et al. 2003; Bastian, Covey & Meyer 2010), indicating that determinations of the IMF are unable

* Based on observations collected at the European Organization for Astronomical Research in the Southern hemisphere, Chile (programme 091.D-0804), and observations obtained at the MMT Observatory, a joint facility of the University of Arizona and the Smithsonian Institution.

† E-mail: kwardduo@asu.edu

to probe the universality or diversity of star formation. An alternate approach is the analysis of binary populations, since observed differences in binary populations in independent regions suggest differences in the star formation process (e.g. Goodwin 2010; King et al. 2012a,b; Parker & Meyer 2014). A well-characterized field M-dwarf binary sample is essential for comparison with the full membership of star-forming regions.

In addition to the importance for understanding the products and process of star formation, companion stars may critically impact planet formation and evolution. A companion star is expected to gravitationally truncate a protoplanetary disc to a radius of approximately one-third the binary star orbital semi-major axis (Artymowicz & Lubow 1994), thereby limiting the amount of material and the region over which planet formation can occur. Determining the population of companions with separations comparable to or less than typical disc sizes of ~ 100 au (Andrews et al. 2009) is particularly important in considering dynamical effects on the disc, and nearby stars are ideal targets to probe the disc-sized separation range with imaging.

Once planets form, the presence of even a distant companion can alter the dynamics of a planetary system through the Kozai mechanism (Kozai 1962; Lidov 1962). There are indications that some exoplanet systems have been impacted by this dynamical effect (e.g. Wu & Murray 2003), and simulations of early dynamical interactions in star-forming regions have shown that the Kozai mechanism could be induced in up to 20 per cent of field binaries (Parker & Goodwin 2009), subsequently affecting a sizable fraction of the exoplanet population. Determining the binarity of the field population and comparing with primordial binary distributions are critical to determining the fraction of stable stellar systems amenable to hosting planets, as demonstrated recently for G-dwarfs (Parker & Quanz 2013). As the population statistics of exoplanets around low-mass stellar hosts are explored, an understanding of the stellar companions to M-dwarfs represents an important comparison and environmental factor.

Existing M-dwarf binary surveys have sample sizes or selection criteria that impact the interpretation of the population statistics of the companions. The benchmark survey of nearby M-dwarfs by Fischer & Marcy (1992) remains the only survey with complete separation coverage by combining radial velocity, speckle, and direct imaging, however the sample size is restricted to fewer than 65 stars per technique, resulting in large uncertainties on the distributions of mass ratio and separations relative to surveys of more massive primaries (e.g. Raghavan et al. 2010; De Rosa et al. 2014). While more recent M-dwarf surveys include larger samples, the selection criteria include a mixed collection of distances (often based on photometry) or activity indicators, and only the single technique of adaptive optics (AO) or lucky imaging was employed, so the separation range coverage was limited (Bergfors et al. 2010; Janson et al. 2012).

To develop comprehensive population statistics on the companions to a large-scale volume-limited sample of nearby low-mass stars, we have conducted a binary survey of 245 K7-M6 dwarfs within 15 pc based on *Hipparcos* parallaxes. By combining archive and new observations with high-resolution and wide-field imaging, the study spans three-and-a-half orders of magnitude in separation. In Section 2, the definition and characteristics of the M-dwarfs in Multiples (MinMs) sample are presented. In Section 3, the new and archival observations are described. The data reduction and analysis method are explained in Section 4. The results and discussion are explored in Section 5. Finally, Section 6 reports a summary of the results.

2 SAMPLE

2.1 Sample selection

The MinMs sample is derived from the new reduction of the *Hipparcos* catalogue (van Leeuwen 2007). We selected all stars with parallaxes greater than $\pi \geq 66.67$ mas, corresponding to stars located within a distance limit of $D \leq 15$ pc. In order to obtain precise distances and absolute magnitudes, stars with parallax errors larger than $\sigma_\pi/\pi \geq 0.10$ were excluded from the sample. Johnson V -band magnitudes were obtained from the original *Hipparcos* catalogue (Perryman et al. 1997), which comprises ground- and space-based photometry with uncertainties ≤ 0.08 mag, and K_S -band magnitudes were obtained from the Two Micron All Sky Survey (2MASS; Skrutskie et al. 2006), providing $V - K_S$ colours.

Stars with K_S magnitudes with significant errors and/or poor quality flags ('X', 'U', or 'F') were excluded from the sample selection. We also excluded five stars identified as companions to earlier spectral types, as given in the Washington Double Star catalogue (WDS; Mason et al. 2001) and confirmed by common proper motion (CPM; see Section 4.3): HIP 83599, HIP 26801, HIP 42762, HIP 45343/HIP 120005. The parallax and photometric quality criteria provided an all-sky, volume-limited sample of 449 stars of over a wide range of spectral types, as shown in the colour-magnitude diagram (CMD) in Fig. 1. M-dwarfs were then selected from this sample by adopting a colour cut of $V - K_S > 3.65$, corresponding to spectral class M0 and later (Kenyon & Hartmann 1995). Additionally, only stars with $M_V > 8$ were included to remove any possibility of contamination from evolved stars. The combined parallax, colour, and magnitude criteria define a total sample of

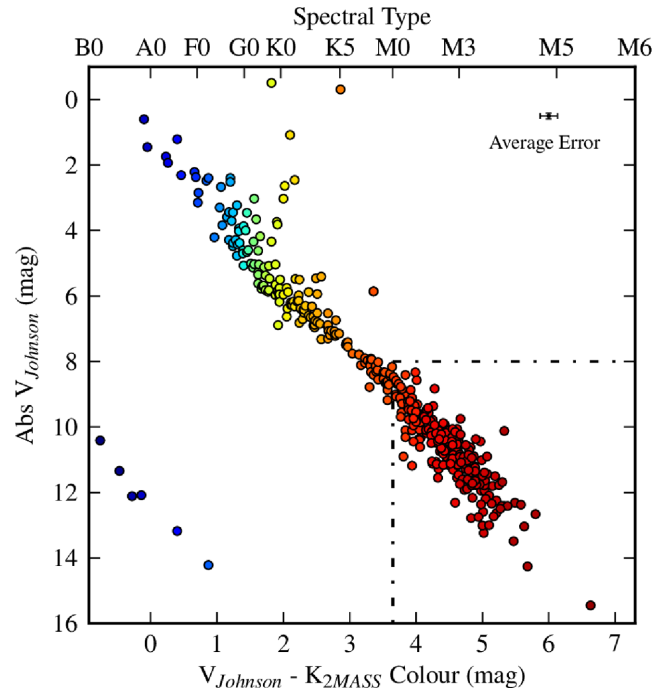


Figure 1. Colour-magnitude diagram of all 449 stars within 15 pc meeting our *Hipparcos* parallax error ($\sigma_\pi/\pi \leq 10$ per cent) and photometry criteria. The colour and magnitude criteria used to select our sample of 245 M-dwarfs ($V - K_S \geq 3.65$, $M_V > 8$) are shown with dash-dotted lines enclosing our sample space on the CMD. The stars are colour-coded by spectral type, with the paucity of lowest-mass/reddest M-dwarfs at far distances indicative of the sensitivity limit of the *Hipparcos* catalogue. An example of the typical error bar size is shown in the upper right corner of the figure.

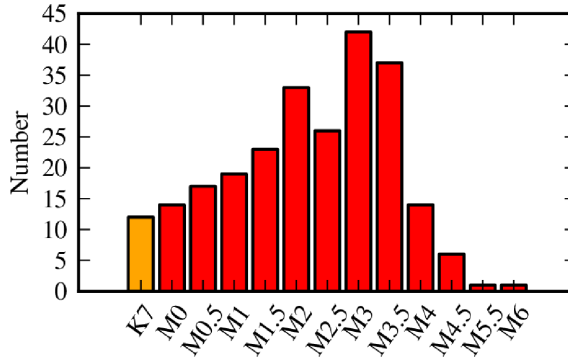


Figure 2. The spectral type distribution of the 15 pc volume-limited 245 M-dwarf sample. The sample has a higher proportion of early-type M-dwarfs, owing to the sensitivity limit of the *Hipparcos* instrument. One star in the sample, HIP 117828, has a spectral type of ‘Ma’ as classified by Houk & Cowley (1975) but lacks a more recent classification, and is not included in this histogram.

245 K and M-dwarfs, of which over 95 percent are M spectral types.

2.2 Sample properties

The spectral type distribution of the sample is shown in Fig. 2, with the majority (94 per cent) of the sample spectral type classifications obtained from the Palomar/MSU Nearby Star Spectroscopic Survey (PMSU, Reid, Hawley & Gizis 1995; Hawley, Gizis & Reid 1996). The spectral types of the remaining stars without PMSU classifications were obtained from the SIMBAD data base (Wenger et al. 2000; individual references listed in Table 1). Uncertainties on the colours and a spread in metallicity led to the inclusion of 12 K7 spectral types, as shown in Fig. 3 (discussed in further detail in Section 5.2). Given the limiting magnitudes of the *Hipparcos* catalogue of $V = 12.4$ (ESA 1997), the latest M spectral types were too faint to be detected, leading to the larger frequency of early M-dwarfs in the sample. The distance distribution of the sample is shown in Fig. 3. The mass of each primary was estimated from theoretical mass–magnitude relations (Baraffe et al. 1998), with the resulting distribution shown in Fig. 4.

3 DATA SOURCES AND ACQUISITION

The MiMMs survey made use of new and archival AO observations and archival digitized photographic plates to detect companions to M-dwarfs. The AO data provide the capacity to search for companions at high angular resolution, while the plate data provide a complementary widefield search space. Combined, the two detection techniques provide nearly continuous angular separation coverage for companions from ~ 0.1 arcsec to ~ 10 arcmin. In this section, we describe the archival data origins and the newly obtained AO observations.

3.1 Archival high-resolution imaging data

To search for companions at projected separations of ~ 1 –100 au from their host stars, we queried all publicly available high-resolution and AO archives. Of the 245 star total sample, 181 stars had previous high-resolution AO imaging. We obtained archival near-infrared AO imaging data from the following instruments/facilities: NAOS-CONICA (NaCo: Nasmyth Adaptive Optics System Near-Infrared Imager and Spectrograph, Lenzen et al.

Table 1. The 245 K7–M6 dwarf sample within 15 pc[†].

HIP	α (J2000.0)	δ (J2000.0)	μ_α (mas yr $^{-1}$)	μ_δ (mas yr $^{-1}$)	V (mag)	J (mag)	H (mag)	K_S (mag)	π (mas)	Distance (pc)	SpTy.	[Fe/H] (dex)	Ref.
428	1.295368	45.786567	869.7	-151	9.95	6.704 ± 0.021	6.098 ± 0.024	5.853 ± 0.018	88.88 ± 1.42	11.25 ± 0.18	M1	-0.01	2
439	1.351784	-37.357361	5634.4	-2336.4	8.56	5.328 ± 0.019	4.828 ± 0.076	4.523 ± 0.017	230.42 ± 0.90	4.34 ± 0.02	M1.5	-0.45	1
1242	3.873033	-16.133639	-32.1	-149.7	11.49	7.215 ± 0.019	6.712 ± 0.034	6.390 ± 0.016	200.53 ± 9.41	4.99 ± 0.23	M4		
1475	4.595353	44.022949	2887.5	408.9	8.09	5.252 ± 0.264	4.476 ± 0.200	4.018 ± 0.020	278.76 ± 0.77	3.59 ± 0.01	M3.5	-0.26	2
2552	8.122664	67.235616	1741.1	-246.8	10.27	6.844 ± 0.023	6.268 ± 0.021	6.037 ± 0.023	99.35 ± 2.17	10.07 ± 0.22	M2	-0.28	3
3937	12.63845	24.816829	223.7	-40.9	12.01	7.951 ± 0.023	7.350 ± 0.015	7.119 ± 0.020	84.42 ± 4.65	11.85 ± 0.65	M3.5		
4569	14.616383	-27.857032	1293.4	-298.9	11.77	7.763 ± 0.023	7.203 ± 0.051	6.892 ± 0.021	80.95 ± 3.21	12.35 ± 0.49	M3.5		
4856	15.6343	71.679816	1745.3	-380.9	9.98	6.301 ± 0.034	5.699 ± 0.049	5.449 ± 0.017	121.41 ± 1.25	8.24 ± 0.08	M3		
4872	15.661952	62.345041	730.3	88.4	9.56	6.230 ± 0.021	5.582 ± 0.024	5.371 ± 0.020	100.40 ± 1.52	9.96 ± 0.15	M1.5	0.15	2

References (metallicities). – ¹ Neves et al. (2014); ² Gaidos & Mann (2014); ³ Rojas-Ayala et al. (2012); ⁴ Newton et al. (2014)

Spectral type references for targets without PMSU classifications. – ^a Gray et al. (2006); ^b Browning et al. (2010); ^c Torres et al. (2006); ^d Poveda et al. (2009); ^e Koen et al. (2010); ^f Houk & Cowley (1975).

[†]Table 1 is published in its entirety in the electronic edition of the journal. A portion is shown here for guidance regarding its form and content.

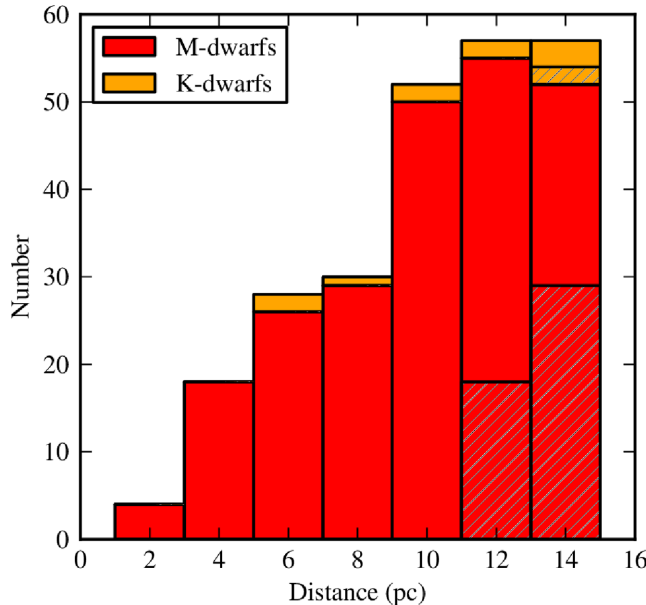


Figure 3. The distance distribution of the 15 pc volume-limited 245 star sample. The darker, hatched portion of the histogram represents stars without new and/or archival AO data. All of the K- and M-dwarfs in our sample up to 11 pc (189 targets) have high-resolution imaging data, covering projected separations of $\sim 1\text{--}100$ au. Archival digitized photographic plates were analysed for the entire sample (both darker and lighter solid regions), covering projected separations of $\sim 100\text{--}10\,000$ au.

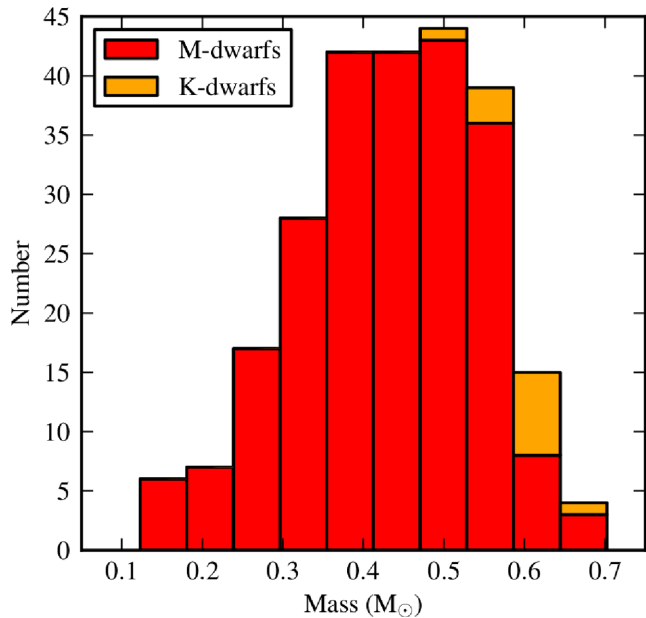


Figure 4. The distribution of primary masses for the targets within the sample. The masses were estimated by comparing the absolute K_S magnitude of each target with theoretical solar-metallicity mass–magnitude relations (Baraffe et al. 1998).

2003; Rousset et al. 2003) on the Very Large Telescope (VLT); the AOB/PUEO KIR camera (Doyon et al. 1998) on the Canada–France–Hawaii Telescope (CFHT); and CIAO (Coronagraphic Imager; Murakawa et al. 2003, 2004), HiCIAO (High Contrast Instrument for the Subaru Next Generation Adaptive Optics; Hodapp et al. 2008), and IRCS (Infrared Camera and Spectrograph;

Tokunaga et al. 1998; Kobayashi et al. 2000) on Subaru. Table 2 provides a summary of the telescopes and instruments used to obtain the first epoch data. Archive AO data from three sources – CFHT, VLT, and Subaru – combined with new AO images from MMT, covered 196 of the 245-star MinMs sample. Some of the targets have additional archive data, and the data used in this study were selected based on the availability of unsaturated images, with preference given to the three instruments that observed the largest number of targets in archives. Existing observations and their corresponding calibration files were downloaded from the Canadian Astronomy Data Centre, the European Southern Observatory Science Archive Facility, and the Subaru-Mitaka-Okayama-Kiso Archive System (Baba et al. 2002). Detailed information on the observations, including observation, filter, exposure time, date, programme ID and project PI for each target are provided in Table 2.

3.2 New AO observations

In addition to the existing archival observations of the sample, 32 dedicated observations – 16 new first-epoch imaging, and 16 follow-up second epoch imaging – were obtained. New and follow-up observations for 26 stars were taken in March, May, and September of 2013 using the Arizona Infrared imager and Echelle Spectrograph (ARIES; McCarthy et al. 1998) at the MMT Observatory. We also obtained second-epoch confirmation imaging for an additional six southern targets in our sample from 2013 March through 2013 September with VLT/NaCo (programme ID: 091.D-0804). The details of these observations are listed in Table 3. When possible, follow-up second-epoch images were obtained with similar configurations as the discovery epochs. New observations of targets from the MinMs sample were taken in the K_S filter, as the majority of the existing archival observations (64 per cent) were taken in K_S band.

3.3 Archival photographic plates

In order to extend the AO imaging survey with a wider search for companions at separations from ~ 100 to $10\,000$ au, we used the SuperCOSMOS Sky Survey Science Archive (Hambly et al. 2001) to obtain scans of plates from the UK Schmidt (UKST), ESO Schmidt, and Palomar Oschin Schmidt (POSS) sky surveys for the full 245-star sample. The archival plates provide multiple epochs of observation for each target, taken with the $BVRI$ filters at a pixel scale of 0.67 arcsec pixel $^{-1}$. With time baselines spanning from 10 to 50 years between the initial and final epochs, and the extremely high proper motions of the targets in our sample (sample median proper motion of 0.63 arcsec yr $^{-1}$), it is possible to search for CPM pairs. Mosaics of the plates were made to provide a search radius around each M-dwarf, and the mosaic dimensions correspond to a projected separation of $10\,000$ au from each primary star.

4 DATA REDUCTION AND ANALYSIS

4.1 Adaptive optics data

4.1.1 Image reduction

For all AO data sets, standardized data reduction techniques of dark subtraction, bad pixel rejection, flat-fielding, and sky subtraction were applied. Unsaturated science frames were aligned by fitting a Gaussian to the point spread function (PSF) of the primary in each image to determine the centroid and align on the peak of that fit. After alignment, the individual frames were median combined to

Table 2. High-resolution imaging data[†].

HIP	Telescope	Instrument	Filter	Exp. time (s)	Programme ID	PI	UT date
428	CFHT	PUEO/KIR	Bry	6	00BF25	Perrier-Bellet	2000-08-21
439	VLT	NaCo/S13	NB1.64	8	072.C-0570(A)	Beuzit	2003-12-08
1242	VLT	NaCo/S13	NB1.64	0.7	072.C-0570(A)	Beuzit	2003-12-10
1475	CFHT	PUEO/KIR	Fe II	0.5	99IID409	Ménard	1999-08-25
2552	CFHT	PUEO/KIR	Bry	10	07AF12	Forveille	2007-01-28
3937	CFHT	PUEO/KIR	H	10	h8	Jewitt	2000-08-19
4856	CFHT	PUEO/KIR	H ₂ (v=1-0)	4	03BD2	Forveille	2003-10-16
4872	CFHT	PUEO/KIR	Fe II	2	97IIF28	Beuzit	1997-12-27
5496	VLT	NaCo/S13	H	5	382.D-0754(A)	Bean	2008-10-17
5643	CFHT	PUEO/KIR	K	1	00BH12	Roddier	2000-12-12

[†]Table 2 is published in its entirety in the electronic edition of the journal. A portion is shown here for guidance regarding its form and content.

Table 3. AO observations summary.

Telescope	Instrument	First epoch	Second epoch	Filters (bandpass)	Pixel scale (mas pixel ⁻¹)	Unique programmes
CFHT	AOBIR	94	23	JHK	38	34
VLT	NaCo	79	24	JHKL'	13, 27, 54	31
MMT	ARIES	16	10	K	20, 40	2
Subaru	CIAO	5	0	HK	22	4
Subaru	HiCIAO	1	0	H	10	1
Subaru	IRCS	2	0	K	21	2

form a final reduced science image for each of the 196 M-dwarfs with new or archival AO imaging. The typical combined integration time for a given target was ~ 60 s, with individual exposure times ranging from 0.3 to 15 s.

4.1.2 Sensitivity and completeness estimation

Given the heterogeneous origins of the AO data sets, the contrast limits of the observations differ between targets. To assess the sensitivity of the full sample to detecting companions over a range of separations, we generated contrast curves for each target. The ensemble of contrast values was used to estimate the completeness of the study. For each reduced, combined science image, the contrast as a function of separation was measured by first determining the standard deviation of the background level within a five pixel annulus over a range of separations from the primary star, and then calculating the corresponding magnitude difference between the peak value of the primary star PSF and 3σ over the background, as tabulated in Table A1 (Appendix). The maximum angular separation at which a companion could be detected in the image was considered to be the limit where 95 per cent of the pixels within that radius were within the boundaries of the image field of view.

4.1.3 Companion detection, photometry and mass estimates

For each K7-M6 dwarf, the reduced, combined image was carefully visually inspected for candidate stellar companions. Previous comparisons with automated detection procedures have verified the reliability of visual inspection (Metchev & Hillenbrand 2009), and we repeated the inspection multiple times for each target on both individual and combined frames. Examples of detected companions are shown in Fig. 5. After identification, the fluxes of the candidates

and their host stars were measured using aperture photometry in IDL. An aperture with radius 2.5 times the average full width at half-maximum (FWHM) was chosen in order to measure the total flux associated with the star or candidate in question, with the sky contribution subtracted by defining an annulus of radius three to nine times the FWHM outside of this aperture. Measurement of the flux ratio between the primary and companion allowed us to derive the magnitude difference of the two objects; any stars unresolved in the 2MASS photometry (with $\Delta m < 4$ and $\rho < 10$ arcsec) were corrected for the individual contributions from each of the stellar components (De Rosa *et al.* 2011). The centroids of the primary target and candidate companion were found with a Gaussian fit, providing an accurate measurement of the pixel separation between the pair of objects. This was converted to an angular separation between the objects using the known pixel scales of the instruments, given in Table 3. We converted angular separation using the *Hipparcos* parallax-based distance measurements into projected separation in au.

To determine the masses of stellar components in a system, we utilized the low-mass, solar-metallicity evolutionary models of Baraffe *et al.* (1998), assuming a standard field star age of 5 Gyr. Using the absolute magnitudes of the primaries, these models were also applied to the sensitivity curves calculated in Section 4.1.2 to determine the completeness of the AO imaging in terms of detectable companion mass.

4.2 Archival plate analysis

4.2.1 Companion detection algorithm

Detection of comoving companion candidates within the mosaicked plates was performed by measuring all objects within the plates using Source Extractor (Bertin & Arnouts 1996). With these

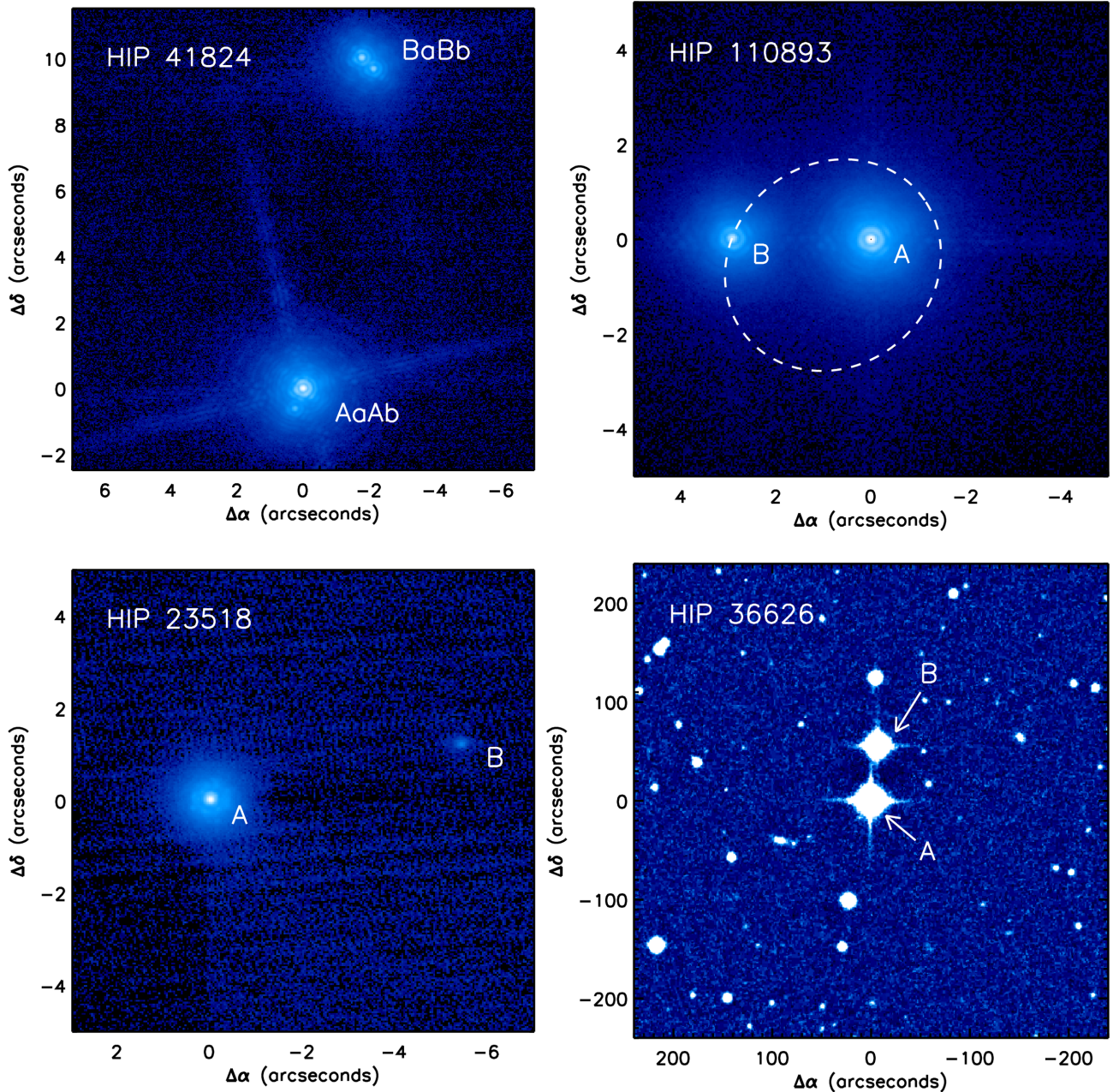


Figure 5. Four of the companions identified or recovered within this study. Top left: a CFHT/AOBIR image of the hierarchical quadruple system HIP 41824 (CU Cnc), originally discovered by Beuzit et al. (2004), which consists of four M-dwarfs in an ϵ Lyr-like configuration (e.g. Tokovinin 2008). Top right: a CFHT/AOBIR image of the HIP 110893 binary system. The measured separation and position angle is consistent with the orbital fit given in Heintz (1986), which is overplotted (white dashed curve). Bottom left: an MMT/ARIES image of the newly discovered binary companion to HIP 23518. With an estimated mass of $0.08 M_{\odot}$, HIP 23518 B is at the canonical stellar/substellar boundary. Bottom right: a photographic plate from the Palomar telescope, obtained from the SuperCOSMOS Sky Survey, showing the two components of the wide HIP 36626 (VV Lyn) binary system (Worley 1962).

parameters, we derived the proper motion for each object with respect to the stationary background stars in the field. An object was considered a CPM candidate if its measured proper motion with respect to the background field stars was within 5σ of the *Hipparcos*-measured proper motion of the primary. These candidates were then visually inspected by blinking the plates from different epochs to eliminate false positives, such as artefacts from the plate scanning process. As noted in Section 2, any stars within our *Hipparcos*-selected sample which were themselves companions to earlier spectral types were excluded from our analysis and statistics.

4.2.2 Sensitivity and completeness estimation

To determine the sensitivity of the plate images, we calculated radial contrast curves using the same method applied to the AO data, starting at an annulus of five pixels from the centroid position of the primary. The *B*-band images were chosen for the sensitivity estimates as they provided the highest resolution and minimal saturation of the primary. The depth of the plates provided many faint unassociated objects within the field, and the catalogued magnitudes of these unassociated objects corresponded to magnitudes far below the substellar limit for associated objects. Given the depth of

the plates, any stellar companions were readily identified by visual inspection. To determine the minimum detection separation for a stellar companion at the bottom of the main sequence, the expected *B*-band magnitude of a $0.08 M_{\odot}$ star was estimated from models, and the corresponding level of pixel counts in the plate was determined by matching to a star in the PPMXL catalogue (Roeser, Demleitner & Schilbach 2010) with the same apparent magnitude.

4.2.3 Photometry and mass estimates

For each comoving companion identified within the plate images, angular separations and magnitude differences from the primary M-dwarfs were derived from the 2MASS catalogue astrometry and K_S -band photometry. As in the AO data analysis, the magnitude differences between the components were converted into component masses using 5 Gyr isochrones (Baraffe et al. 1998). The identified CPM companions were then cross-referenced against binary component identifications in the WDS catalogue (Mason et al. 2001). Detected companions were also cross-checked against known catalogues of white dwarf/M-dwarf pairs (Silvestri et al. 2001) and white dwarf catalogues (McCook & Sion 1999) to remove any contamination from systems with known higher-mass companions.

4.3 Astrometric confirmation

To confirm or reject detected AO and plate CPM candidates, we compared the second-epoch positions with the motion of a background object. The expected motion of a background object was calculated using the *Hipparcos* proper motion and parallax of the primary. In each case, the representative errors in the expected motion of a background object were determined from the first epoch measured uncertainties in position angle and separation. Due to the range of projected separations probed, any resolved companion within the AO images can have measurable orbital motion over the time baseline between the two epochs of observations. In order to estimate a range of possible orbital motions, two scenarios are considered: a face-on, or edge-on circular orbit. For the representative change in the position angle, a face-on circular orbit is used with a semi-major axis equal to the observed projected separation. The period of the orbit is then derived from Kepler's third law, using the masses of the two components given in Table 4, from which the change in the position angle is calculated.

In order to estimate the expected change in the separation for a bound component, an edge-on circular orbit is used. As the projected separation does not correspond to a unique value of the semi-major axis (a), and the rate of change of the separation depends on both a and the location of the companion within the orbit (characterized by the true anomaly, ν), a large number of orbits were simulated. For a given projected separation (a_{proj}), the four unique values of ν are calculated as

$$\nu = \pm \cos^{-1} \left(\pm \sqrt{\frac{a_{\text{proj}}^2}{a^2}} \right). \quad (1)$$

The limiting case for an edge-on circular orbit is when $a = a_{\text{proj}}$, with ν becoming undefined when $a < a_{\text{proj}}$. For a given value of a , the four values of the true anomaly were increased from ν to $\nu + 2\pi$ over the period determined from Kepler's third law using the masses for each component given in Table 4. The projected separation at each time-step was then calculated as

$$a_{\text{proj}} = a |\cos(\nu)|. \quad (2)$$

As the maximal change in the projected separation as a function of time depends on the true semi-major axis, 10 000 simulations

were run where the value of a was increased from a_{proj} until the maximum value of da_{proj}/dt was reached (typically between $a = 2$ and $3 \times a_{\text{proj}}$). These two representative bounds for the change in projected separation and position angle for a bound companion are shown for four examples given in Figs 6–9, and are shown for all companions which are detected in at least two epochs in Fig. A1 (Appendix). The motion of the candidate companion was compared with the expected motion for a background source, and checked for consistency with the expected change for a bound component, within the uncertainties on position angle and separation available from the second epoch measurement. For the large majority of the historic WDS catalogue measurements, no uncertainties are available for additional epochs.

For three of the targets with companions detected at close angular separations ($\rho \lesssim 0.2$ arcsec) – HIP 36208, HIP 86214, and HIP 114046 – the candidate is not detected within the second epoch. Given the proper motion of the primary, a background object should have been visible in the field in each of these cases. The lack of detection of the companion in the vicinity of the expected location of a background object is used as evidence for the bound nature of the companion, and they are therefore considered bound for the purposes of this study. Continued monitoring of these targets would be required in order to confirm the physical association of these companion by imaging the companion as it passes through apastron.

4.3.1 Assessment of binary sample contamination

We performed two analyses to determine the likelihood of background interlopers contaminating the binary sample. We first determined the background point source density for each of the stars in our sample from the 2MASS catalogue by selecting targets within a 10 000 au radius and within the K_S -band magnitude limits for potential stellar companions, i.e. fainter than the primary star but brighter than the $K_S = 10$ substellar limit. We find a median number of 10.5 candidate sources per 10 000 au radius (median of 3.46×10^{-6} sources arcsec $^{-2}$ in a 5° search radius) for the full MINMs sample. The nearby distances of stars in our sample lead to the large number of background sources within the full companion search radius. While the maximum separation of an AO-detected binary (~ 35 arcsec) has a very low typical probability of background contamination (often $\ll 1$ per cent), the source count method yields significantly higher predictions of the order of a few to 10 per cent for background sources when considering the wider (> 35 arcsec) plate-detected candidates.

In addition to the background source estimation, we determined the likelihood of unassociated field stars sharing similar 2D proper motions with our sample targets, as such systems would also appear as false positives in the binary statistics. Using the online Besançon stellar population synthesis tools (Robin et al. 2003), we generated catalogues of over 12 000 000 stars spanning large fields ($0.0 < \alpha < 360$, $-60 < \delta < +60$), with distance and magnitude limits corresponding to the expected companion properties. As seen in Fig. 10, the extremely high proper motion of our sample leads to small overlap with the synthetic population proper motion distribution (even considering only the magnitude of the total proper motion vector and not the constituent 2D vectors, which would further narrow possible matches). For each star in our full sample, we determined the number of proper motion and K_S -magnitude matches in the synthetic population by selecting on proper motion in both right ascension and declination at various levels of confidence. This yielded the following average numbers of matching synthetic stars over the full sample per target: $1\sigma - 0.08$; $3\sigma - 0.69$; $5\sigma - 1.86$;

Table 4. Confirmed companions – measured and derived properties.

HIP	WDS ^a desig.	UT date	ρ (arcsec)	a_{proj} (au)	θ (deg)	Δm (mag)	Broad-band filter	M_{prim} (M_{\odot})	M_{sec} (M_{\odot})	Epoch
1242	– ^b	2003-12-10	0.21 ± 0.05	1.0 ± 0.3	158.0 ± 1.0	0.93	H	0.15	0.11	1
		2008-06-22	0.19 ± 0.01	0.9 ± 0.0	167.6 ± 3.2	0.58	H	0.18	0.14	2
1475	B	1954-10-03	37.40 ± 0.60	134.1 ± 2.0	59.5 ± 0.1	2.71	K_S	0.42	0.16	1
		1995-10-13	36.28 ± 0.70	130.2 ± 2.0	61.1 ± 0.2	2.71	K_S	0.42	0.16	2
2552	Ab	2001-08-05	0.40 ± 0.10	4.0 ± 1.0	320.0 ± 4.0	1.28	K_S	0.40	0.21	1
		2007-01-29	0.39 ± 0.02	3.9 ± 0.2	72.5 ± 1.7	1.21	K_S	0.46	0.25	2
2552	B	2001-08-05	4.01 ± 0.09	40.0 ± 1.0	177.1 ± 0.2	1.35	K_S	0.40	0.22	1
		2007-01-29	3.99 ± 0.06	40.2 ± 0.6	171.8 ± 1.1	1.35	K_S	0.40	0.22	2
3937	–	2000-08-19	1.68 ± 0.09	20.0 ± 2.0	322.3 ± 0.5	0.61	H	0.26	0.19	1
		2013-09-18	1.03 ± 0.18	12.1 ± 2.1	319.8 ± 0.7	0.61	K_S	0.26	0.19	2
4872	B	1952-09-15	296.40 ± 0.60	2,952.0 ± 45.0	75.5 ± 0.3	0.61	K_S	0.56	0.2	1
		1995-09-14	295.50 ± 0.60	2,943.5 ± 45.0	75.5 ± 0.3	0.61	K_S	0.56	0.2	2
5496	–	2003-12-09	0.07 ± 0.07	0.5 ^{+0.6} _{-0.5}	165.0 ± 2.0	0.44	H	0.43	0.36	1
		2008-10-17	0.09 ± 0.01	0.7 ± 0.1	73.7 ± 1.8	0.26	H	0.52	0.45	2
9724	–	2003-12-09	0.52 ± 0.05	4.8 ± 0.5	102.1 ± 0.4	3.25	H	0.47	0.11	1
		2013-07-03	0.62 ± 0.01	5.7 ± 0.5	102.1 ± 0.4	3.25	H	0.47	0.11	2
10617	–	1986-09-03	105.50 ± 0.60	1,511.0 ± 68.0	312.1 ± 0.1	2.11	K_S	0.40	0.27	1
		1997-11-22	105.60 ± 0.60	1,512.1 ± 68.0	312.1 ± 0.1	2.11	K_S	0.40	0.27	2
15220	B	1954-01-28	6.75 ± 1.00	97.2 ± 15.0	12.9 ± 5.0	0.07	K_S	0.50	0.49	1
		1995-11-12	5.65 ± 1.00	81.2 ± 15.0	6.0 ± 5.0	0.07	K_S	0.50	0.49	2
22738	–	2004-09-23	7.65 ± 0.05	85.0 ± 2.0	314.7 ± 0.1	0.72	H	0.36	0.25	1
		2012-08-24	7.47 ± 0.56	83.1 ± 0.2	314.7 ± 0.1	0.71	H	0.35	0.25	2
23452	B	2002-09-18	0.81 ± 0.09	6.9 ± 0.8	285.4 ± 0.7	1.30	K_S	0.59	0.37	1
		2014-01-13	0.89 ± 0.18	7.6 ± 1.6	335.4 ± 4.8	1.30	K_S	0.59	0.37	2
23518	★ ^c	2013-09-18	5.60 ± 0.20	76.0 ± 3.0	279.5 ± 0.3	4.81	K_S	0.54	0.08	1
		2014-01-10	5.58 ± 0.20	76.1 ± 2.4	279.1 ± 0.3	4.81	K_S	0.54	0.08	2
23932	–	2003-03-16	0.06 ± 0.05	0.6 ± 0.5	30.0 ± 4.0	0.10	K_S	0.43	0.41	1
		2011-02-16	0.07 ± 0.05	0.7 ± 0.5	44.4 ± 5.5	0.10	K_S	0.43	0.41	2
28368	–	1954-01-05	163.10 ± 0.60	2,208.0 ± 50.0	119.4 ± 0.6	0.20	K_S	0.53	0.22	1
		1996-12-10	162.50 ± 0.60	2,199.6 ± 50.0	119.5 ± 0.6	0.20	K_S	0.53	0.22	2
29316	B	2004-01-07	1.72 ± 0.09	19.0 ± 1.0	30.1 ± 0.2	1.50	K_S	0.45	0.22	1
		2013-09-18	0.58 ± 0.18	6.3 ± 1.9	52.5 ± 1.1	1.50	K_S	0.45	0.22	2
30920	B	2006-04-11	1.37 ± 0.05	5.6 ± 0.2	47.4 ± 0.2	1.24	K_S	0.21	0.1	1
		2009-03-28	1.07 ± 0.01	4.4 ± 0.0	74.6 ± 0.3	1.61	K_S	0.24	0.13	2
31293	–	1977-02-10	23.00 ± 0.60	207.3 ± 7.0	35.3 ± 0.3	0.76	K_S	0.45	0.32	1
		1989-12-31	23.22 ± 0.60	209.4 ± 7.0	34.0 ± 0.3	0.76	K_S	0.45	0.32	2
33142	–	2002-09-12	0.30 ± 0.10	3.0 ± 1.0	250.0 ± 3.0	0.47	H	0.32	0.25	1
		2005-04-27	0.19 ± 0.01	1.9 ± 0.1	160.5 ± 3.9	0.47	H	0.32	0.25	2
33499	– ^f	2003-12-08	0.83 ± 0.05	6.6 ± 0.4	282.9 ± 0.3	0.01	H	0.24	0.24	1
35191	–	2000-02-25	0.06 ± 0.05	0.7 ± 0.6	154.0 ± 6.0	0.32	J	0.39	0.34	1
		2003-12-08	0.06 ± 0.01	0.8 ± 0.1	334.5 ± 6.0	0.32	J	0.39	0.34	2
36208	★ ^e	2003-12-11	0.17 ± 0.05	0.6 ± 0.2	327.0 ± 4.0	1.07	H	0.24	0.14	1
36626	Ab	2000-04-20	0.70 ± 0.10	8.0 ± 1.0	201.0 ± 4.0	1.87	K_S	0.51	0.21	1
		2013-09-18	1.53 ± 0.01	18.1 ± 0.1	194.4 ± 0.6	1.87	K_S	0.51	0.21	2
36626	B	1955-02-13	38.40 ± 0.60	456.0 ± 20.0	354.2 ± 0.1	3.82	K_S	0.51	0.39	1
		1998-12-28	38.04 ± 0.60	451.5 ± 20.0	353.2 ± 0.1	3.82	K_S	0.51	0.39	2
41824	Ab	1999-02-27	0.67 ± 0.09	7.0 ± 1.0	157.2 ± 0.9	1.48	K_S	0.38	0.11	1
		2007-01-29	0.65 ± 0.09	7.2 ± 1.0	169.9 ± 1.1	1.48	K_S	0.38	0.11	2
41824	Ba	1999-02-27	10.17 ± 0.09	113.0 ± 10.0	348.6 ± 0.1	1.74	K_S	0.38	0.17	1
		2007-01-29	10.32 ± 0.09	114.2 ± 10.0	348.5 ± 0.1	1.74	K_S	0.38	0.17	2
41824	Bb	1999-02-27	9.91 ± 0.09	110.0 ± 10.0	346.2 ± 0.1	2.20	K_S	0.38	0.13	1
		2007-01-29	9.58 ± 0.09	106.0 ± 10.0	346.0 ± 0.1	2.20	K_S	0.38	0.13	2
46706	–	1997-12-28	0.70 ± 0.10	7.0 ± 1.0	239.0 ± 1.0	0.09	K_S	0.42	0.41	1
		2004-04-05	0.52 ± 0.01	5.2 ± 0.0	49.8 ± 0.3	0.09	K_S	0.54	0.53	2
47620	B	1955-01-26	89.10 ± 0.60	1,096.0 ± 25.0	77.1 ± 0.1	0.60	K_S	0.52	0.46	1
		2000-01-13	88.80 ± 0.60	1,091.8 ± 25.0	77.5 ± 0.1	0.60	K_S	0.52	0.46	2
49969	–	2000-02-19	0.20 ± 0.10	2.0 ± 1.0	253.0 ± 8.0	0.81	H	0.43	0.29	1
		2003-03-18	0.16 ± 0.01	1.9 ± 0.0	61.8 ± 1.4	0.51	H	0.49	0.36	2
54211	B	1955-03-19	30.20 ± 0.60	147.0 ± 3.0	131.1 ± 0.2	4.40	K_S	0.40	0.1	1
		2000-03-14	31.91 ± 0.60	154.7 ± 3.0	126.6 ± 0.2	4.40	K_S	0.40	0.1	2

Table 4 – *continued*

HIP	WDS ^a desig.	UT date	ρ (arcsec)	a_{proj} (au)	θ (deg)	Δm (mag)	Broad-band filter	M_{prim} (M_{\odot})	M_{sec} (M_{\odot})	Epoch
59406	–	1954-04-02	84.70 ± 0.60	$1,066.0 \pm 32.0$	120.9 ± 0.1	1.58	K_S	0.36	0.26	1
		1994-05-18	85.12 ± 0.60	$1,071.7 \pm 32.0$	120.9 ± 0.1	1.58	K_S	0.36	0.26	2
60910	– ^f	2008-02-19	0.07 ± 0.05	0.9 ± 0.7	114.0 ± 5.0	0.70	K_S	0.32	0.22	1
		1997-12-27	0.20 ± 0.10	2.0 ± 1.0	240.0 ± 7.0	0.55	H	0.37	0.28	1
62556	–	2003-03-17	0.32 ± 0.04	3.3 ± 0.4	202.8 ± 4.3	0.55	H	0.37	0.28	2
		2005-05-01	0.28 ± 0.05	3.2 ± 0.6	357.0 ± 1.0	3.26	K_S	0.58	0.12	1
63510	B	2006-05-23	0.24 ± 0.01	2.8 ± 0.1	307.4 ± 4.5	3.71	K_S	0.58	0.12	2
		2005-05-15	19.60 ± 0.20	260.0 ± 9.0	123.1 ± 0.3	0.66	K_S	0.63	0.3	1
65011	B	1990-05-06	17.80 ± 0.20	236.1 ± 9.0	128.9 ± 0.3	0.66	K_S	0.63	0.3	2
		2000-04-20	0.63 ± 0.09	7.0 ± 1.0	107.0 ± 6.0	0.85	K_S	0.67	0.52	1
65026	B	2005-04-27	1.26 ± 0.09	13.5 ± 1.0	94.2 ± 0.2	0.85	K_S	0.67	0.52	2
		1956-04-08	8.90 ± 0.60	123.0 ± 9.0	45.7 ± 2.0	1.36	K_S	0.48	0.22	1
65714	–	1996-04-21	7.65 ± 0.60	106.2 ± 9.0	51.5 ± 2.0	1.36	K_S	0.48	0.22	2
		2002-06-25	2.88 ± 0.09	31.0 ± 1.0	109.9 ± 0.2	3.94	K_S	0.40	0.08	1
71898	–	2004-04-25	2.77 ± 0.01	29.7 ± 0.1	105.8 ± 0.2	3.94	K_S	0.40	0.08	2
		2001-08-06	1.00 ± 0.10	11.0 ± 1.0	116.0 ± 1.0	0.77	K_S	0.29	0.2	1
72896	–	2013-04-19	1.02 ± 0.01	10.3 ± 0.0	93.7 ± 0.0	0.77	K_S	0.37	0.25	2
		2005-06-04	4.92 ± 0.05	47.5 ± 0.9	32.5 ± 0.2	2.66	K_S	0.49	0.09	1
72944	Ba	2006-03-01	4.91 ± 0.01	47.4 ± 0.1	33.4 ± 0.1	2.66	K_S	0.49	0.09	2
		2005-06-04	4.98 ± 0.05	48.1 ± 0.9	32.0 ± 0.2	4.80	K_S	0.49	0.08	1
72944	Bb	2006-03-01	5.01 ± 0.01	48.4 ± 0.1	32.4 ± 0.1	4.80	K_S	0.49	0.08	2
		2003-03-17	1.36 ± 0.09	16.0 ± 1.0	179.2 ± 0.2	2.26	K_S	0.60	0.24	1
73470	–	2005-04-25	1.54 ± 0.01	18.1 ± 0.1	173.0 ± 0.1	2.26	K_S	0.62	0.25	2
		1955-04-23	64.00 ± 0.60	684.0 ± 9.0	12.7 ± 0.1	0.99	K_S	0.66	0.47	1
80018	–	1994-06-18	64.87 ± 0.60	693.2 ± 9.0	13.5 ± 0.1	0.99	K_S	0.66	0.47	2
		2007-05-19	4.92 ± 0.05	41.0 ± 1.0	226.9 ± 0.2	3.02	H	0.38	0.1	1
82817	B	2013-03-29	4.43 ± 0.02	37.0 ± 0.1	226.0 ± 0.1	3.02	H	0.38	0.1	2
		2003-05-29	0.11 ± 0.05	0.7 ± 0.3	275.0 ± 2.0	0.28	H	0.43	0.38	1
82817	C	2005-07-21	0.22 ± 0.01	1.4 ± 0.1	173.8 ± 0.1	0.28	H	0.43	0.38	2
		1954-06-01	73.10 ± 0.60	453.0 ± 16.0	313.8 ± 0.1	0.28	H	0.43	0.2	1
82817	F	1996-04-25	72.75 ± 0.60	450.7 ± 16.0	313.3 ± 0.1	0.28	H	0.43	0.2	2
		1954-06-01	232.50 ± 0.60	$1,440.0 \pm 50.0$	155.4 ± 0.4	4.58	K_S	0.43	0.09	1
84140	B	1996-04-25	232.01 ± 0.60	$1,437.4 \pm 50.0$	155.4 ± 0.4	4.58	K_S	0.43	0.09	2
		1999-04-04	1.11 ± 0.09	6.6 ± 0.6	225.0 ± 0.5	0.01	K_S	0.34	0.34	1
84140	B	2004-04-05	0.25 ± 0.09	1.5 ± 0.5	166.6 ± 5.5	0.01	K_S	0.47	0.47	2
		1951-07-05	15.80 ± 0.60	183.0 ± 11.0	267.3 ± 0.2	1.10	K_S	0.44	0.29	1
84794	–	1996-08-09	16.81 ± 0.60	194.9 ± 11.0	268.7 ± 0.2	1.10	K_S	0.44	0.29	2
		2005-05-01	3.76 ± 0.05	37.0 ± 1.0	325.4 ± 0.3	1.93	H	0.45	0.18	1
86057	–	2007-05-14	3.94 ± 0.05	38.3 ± 1.0	323.7 ± 0.3	1.93	H	0.45	0.18	2
		2005-05-01	0.17 ± 0.05	0.9 ± 0.3	190.0 ± 5.0	1.01	H	0.23	0.14	1
86214	★ ^e	2009-09-01	12.53 ± 0.09	44.7 ± 0.5	170.1 ± 0.1	0.60	K_S	0.26	0.19	1
		2005-05-01	11.98 ± 0.04	42.8 ± 0.1	219.4 ± 0.2	0.60	K_S	0.26	0.19	2
91772	A ^d	1951-07-13	116.60 ± 0.60	$1,020.0 \pm 21.0$	290.2 ± 0.5	1.01	K_S	0.32	0.32	1
		1994-06-12	115.40 ± 0.60	$1,010.1 \pm 21.0$	291.0 ± 0.5	1.01	K_S	0.32	0.32	2
93899	–	2003-07-19	0.08 ± 0.05	0.8 ± 0.6	58.0 ± 6.0	0.80	H	0.34	0.23	1
		2007-05-14	0.16 ± 0.01	1.7 ± 0.0	319.7 ± 1.8	0.80	H	0.41	0.28	2
94349	B	1950-08-12	72.90 ± 0.60	428.0 ± 4.0	149.5 ± 0.5	4.64	K_S	0.49	0.09	1
		1995-08-16	75.36 ± 0.60	442.4 ± 4.0	151.6 ± 0.5	4.64	K_S	0.49	0.09	2
94761	B	2013-09-18	5.60 ± 0.20	76.0 ± 3.0	140.1 ± 0.3	0.71	K_S	0.49	0.37	1
		1976-05-30	41.60 ± 0.60	619.0 ± 47.0	111.0 ± 0.5	1.70	K_S	0.37	0.33	1
99150	–	1996-09-17	41.60 ± 0.60	621.0 ± 47.0	109.4 ± 0.5	1.70	K_S	0.37	0.33	2
		2003-07-21	2.82 ± 0.05	30.0 ± 1.0	171.2 ± 0.2	0.03	K_S	0.54	0.53	1
102141	C	2009-06-01	2.51 ± 0.01	26.8 ± 0.0	159.4 ± 0.6	0.03	K_S	0.66	0.65	2
		2005-05-02	0.19 ± 0.05	1.5 ± 0.4	162.0 ± 1.0	1.12	H	0.27	0.15	1
110893	–	2001-08-04	3.21 ± 0.09	12.9 ± 0.4	103.3 ± 0.2	0.98	K_S	0.27	0.17	1
		2006-05-26	2.96 ± 0.01	11.8 ± 0.1	86.9 ± 0.3	0.98	K_S	0.32	0.2	2
111766	–	2013-05-08	0.78 ± 0.05	10.0 ± 1.0	175.5 ± 0.2	0.24	K_S	0.38	0.34	1
		2005-05-01	0.86 ± 0.01	11.4 ± 0.1	123.0 ± 0.3	0.24	K_S	0.38	0.34	2

Table 4 – *continued*

HIP	WDS ^a desig.	UT date	ρ (arcsec)	a_{proj} (au)	θ (deg)	Δm (mag)	Broad-band filter	M_{prim} (M $_{\odot}$)	M_{sec} (M $_{\odot}$)	Epoch
111802	–	1984-10-15	25.90 ± 0.60	225.0 ± 6.0	351.6 ± 0.1	0.30	K_S	0.60	0.32	1
		1999-08-11	28.07 ± 0.60	244.1 ± 6.0	352.2 ± 0.1	0.30	K_S	0.60	0.32	2
114046	\star^e	2003-12-09	0.07 ± 0.05	0.2 ± 0.2	267.0 ± 3.0	1.21	H	0.44	0.25	1
116132	B	1997-12-25	5.18 ± 0.09	32.0 ± 0.7	93.8 ± 0.3	1.37	K_S	0.35	0.17	1
		2000-08-21	5.28 ± 0.01	32.7 ± 0.0	94.0 ± 0.1	1.37	K_S	0.39	0.2	2

Notes. ^aWDS catalogue component designation.

^bTargets within the WDS catalogue, but without an assigned component designation.

^cNewly confirmed companion without a designation in the WDS catalogue (\star denotes a new companion).

^dHIP 91772 is designated as the ‘B’ component in the WDS catalogue, but has the largest estimated mass of the system.

^eA target for which there is no second epoch detection, but instead a non-detection of a background object (Section 4.3).

^fInstance where second epoch data were not available, but multiple confirmation epochs were obtained from previous WDS measurements.

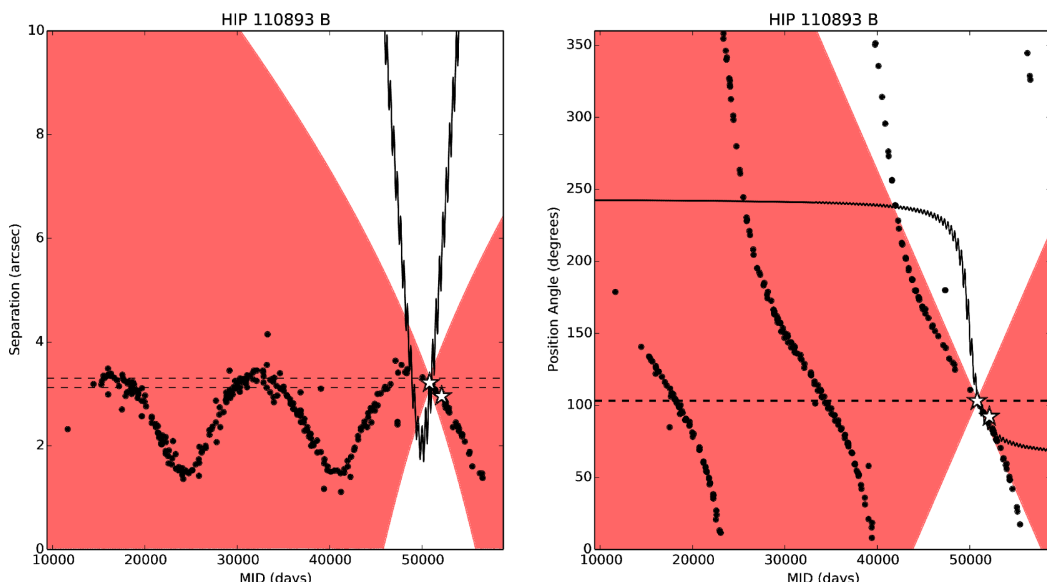


Figure 6. Proper motion diagram showing the change in separation (left panel) and position angle (right panel) between the two components of the HIP 110893 binary system. In both diagrams the measurements presented within this study are denoted by large white stars, with the measurements obtained from the WDS catalogue plotted as small circles (Mason et al. 2001). The dashed horizontal lines denote the upper and lower bounds of the separation and position angle measurement within the first epoch. The expected motion of a stationary background object, given the proper motion and parallax of the M3 dwarf target, is enclosed by the solid black lines. Given the maximal change in separation and position angle for circular orbits calculated in Section 4.3, indicative ranges of allowed separations and position angles are denoted by the red shaded region.

$10\sigma - 8.23$. Of these, each system with a non-zero number of synthetic proper motion matches was selected to check physical association. As shown in Table 5, while these systems may share similar proper motions with some stars in the synthetic sample, the probability of background source contamination from 2MASS in all cases is $\ll 1$ per cent. The combination of these analyses, particularly when coupled with previous orbital parameter measurements, supports the hypothesis of the physical association of all detected wide systems in our survey.

5 RESULTS AND DISCUSSION

5.1 Detected comoving companions and survey completeness

Based on the multi-epoch AO and wide-field imaging data analysis, a total of 47 AO-detected and 20 wide-field-detected physically associated companions were identified in the MiMMs sample (41 systems with one or more companions detected in the close AO data, and 17 systems with one or more companions detected in the

wide plate data, for a total of 58 multiple systems and 187 single stars). Due to some overlap in search space between the two types of data, two different companions were detected independently by the two techniques, resulting in 65 unique comoving companions to the MiMMs sample. Among the AO-detected companions, four are newly identified within this study. The measured astrometry and relative photometry for each of the resolved companions are reported in Table 4, along with the inferred masses of each component derived from an evolutionary model (Baraffe et al. 1998), as described in Section 4.2.3. The 65 companions are distributed in 53 binary systems, three triple systems, and two quadruple systems.

The observed angular separations and magnitude differences for all of the companions are plotted in Fig. 11, and the 3σ median sensitivity of the sample is also shown. The angular separations range from 0.05 to 4.94 arcmin. The magnitude differences measured in one of the infrared filters ranged from $\Delta m = 0.0$ to 5.0. Only stellar companions are considered for this study, so the maximum magnitude difference needed for sensitivity to an M9

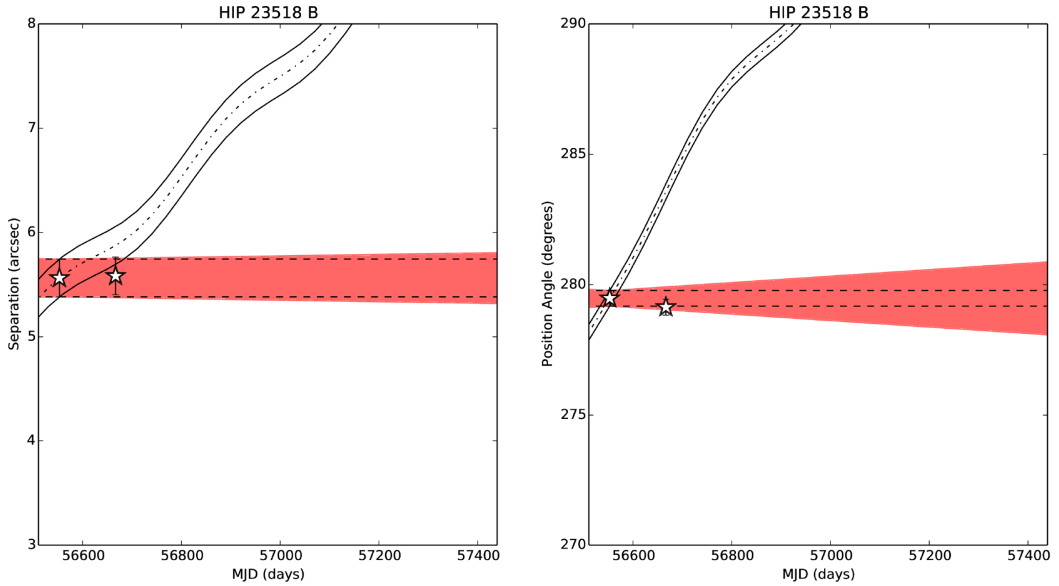


Figure 7. Proper motion diagram for the newly discovered bound companion HIP 23518 B, identified within MMT/ARIES images presented within this study. Symbols, curves, and shading are as with Fig. 6.

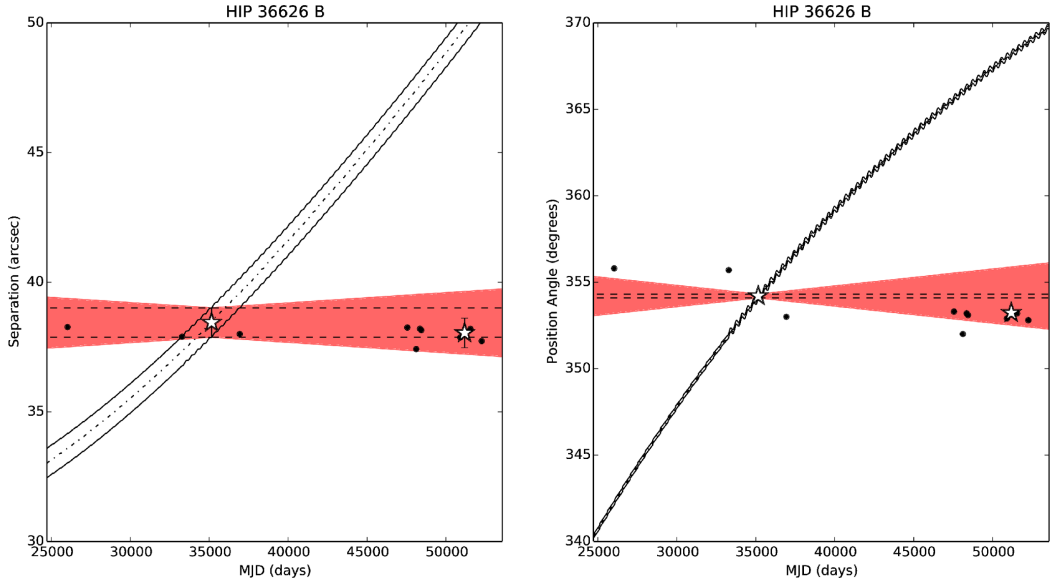


Figure 8. Proper motion diagram for the bound companion HIP 36626 B (VV Lyn B) identified within the photographic plates. Symbols, curves, and shading are as with Fig. 6.

companion ($M_K \sim 10$ mag) to an M0 primary ($M_K \sim 4.5$ mag) is only 5.5 mag at K_S band. The limited dynamic range required to reach the bottom of the main sequence, combined with the sensitive observations, results in a very uniform completeness to stellar companions. Detection limits for all targets are reported in Table A1 (Appendix).

The observational properties are transformed into physical properties of mass and projected separation in Fig. 12. Wider than a few au, the completeness is very high (typically >95 per cent), as shown in Fig. 12. The detected companions are also included in the figure, and comoving objects down to the stellar/substellar limit are identified in the MiNNMs study. The vertical and horizontal dashed lines define the boundaries of the region considered for constructing the distributions of companion separation, secondary mass, and total system mass. The closer pairs (<3 au) are not included in

the population statistics, since the interpretation of the data would be dependent on a large correction factor. A similar plot in terms of mass ratio and projected separation is given in Fig. 13, and the dashed lines delineate the systems included in determining the mass ratio distribution of the MiNNMs sample. Although the sensitivity is very uniform to a companion mass limit of $0.08 M_{\odot}$, the range of target masses makes the lower mass ratio limit of $q \geq 0.2$ for uniform completeness in the mass ratio distribution.

5.2 Comparison of sample properties and binary detections

To determine if any selection biases impacted the study, particularly given the magnitude-limited nature of our survey, we analysed binary occurrence against attributes such as distance, magnitude, and metallicity. To test whether observed binaries were consistent

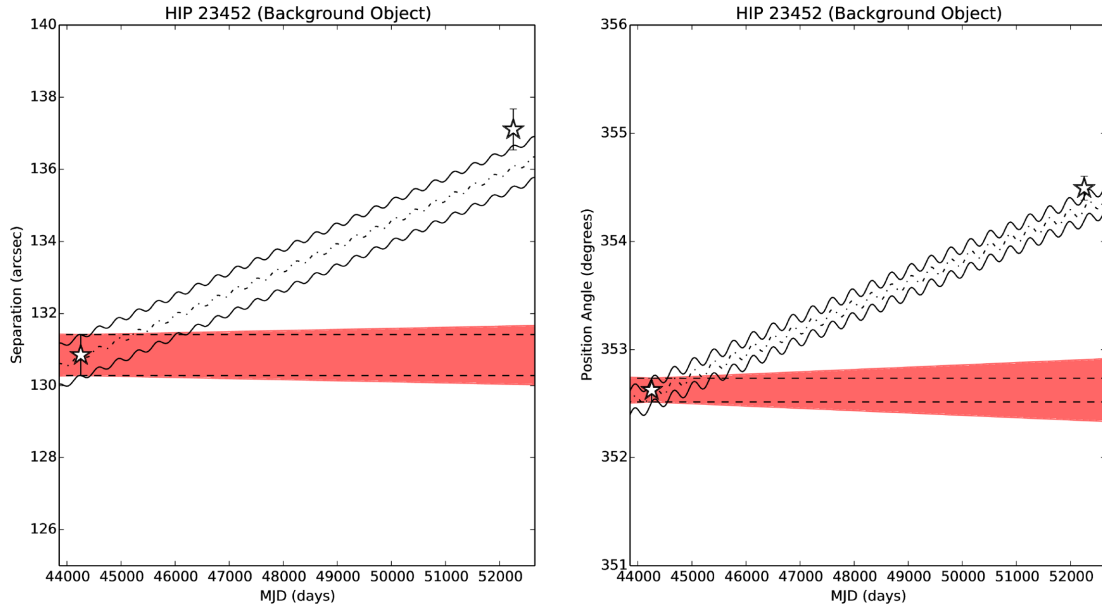


Figure 9. Proper motion diagram for a background object within the vicinity of HIP 23452 identified within the photographic plates. Symbols, curves, and shading are as with Fig. 6.

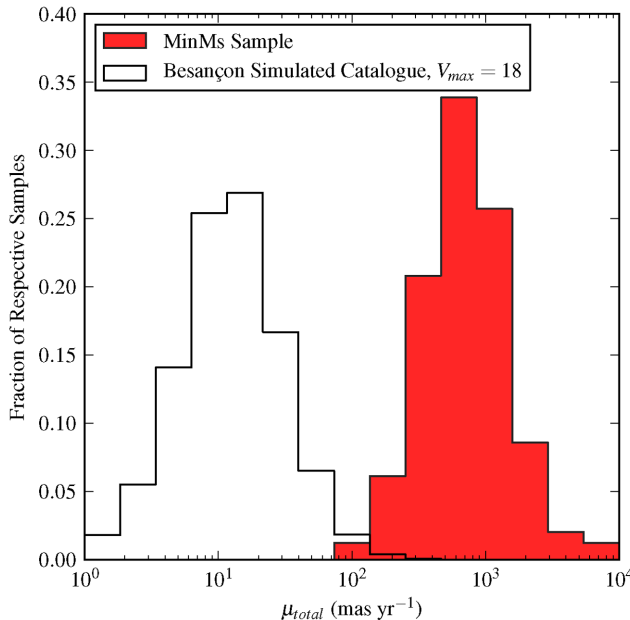


Figure 10. The relative proper motion distribution fractions for the MinMs sample and a comparable synthetic Besançon stellar catalogue (Robin et al. 2003), generated with similar sample properties.

with being drawn randomly from the survey sample, all systems were rank-ordered by a given attribute and the binaries were plotted to create a cumulative distribution function, which could then be compared against a random distribution. This was performed using a method similar to calculating the Gini coefficient, a widely used statistic in economics measuring wealth distribution within societies (Gini 1955). For each system attribute, the area underneath the binary distribution, normalized to 0.5, was calculated. The error on the area was estimated with a Monte Carlo simulation of 10 000 random distributions, each with the same number of binaries in the

same number of total targets. In this study, the 58 multiple systems within 245 total systems lead us to an expected area of 0.5 ± 0.03 .

The comparisons for the systems in our survey are shown in Fig. 14 for the distances of the systems, and Fig. 15 for the magnitude distribution of the target sample. For the distance distribution, we find the area beneath the binary distribution to be 0.54, slightly over 1σ away from the expected area value. This may be seen in a slight overabundance of binaries near rank order 0.5, corresponding to systems at ~ 8 pc, but is still consistent with a random distribution, and so the sample does not appear to be significantly biased towards systems at closer or further distances. Similarly, for the V-band magnitude distribution in Fig. 15, the area was also 0.54, and is again consistent with a random underlying distribution. Similar comparisons were performed for the binaries within only the 196-star AO subsample, with area values of 0.49 for the distance distribution and 0.52 for the magnitude distribution, which are also consistent with selection from a random distribution.

Using literature values for the 124 stars within our sample with previous metallicity measurements (Table 1), subsamples of the binaries and single stars were also compared with the same technique. With 20 observed multiple systems within the 124 star subsample with metallicity measurements, the expected integrated area of the binary distribution function is 0.5 ± 0.06 . With an observed value of 0.45, the survey also appears consistent with a random distribution with respect to stellar metallicity, and suggests no dependence of binarity upon the system metallicity. With very few measurements of extremely metal-poor or metal-rich stars within our sample, no binaries were detected at extreme metallicities, underscoring the utility of additional sample metallicity and age estimations in determining robust statistics for various population subsamples.

5.3 Projected separation distribution

The separation range of 3 au defined from the survey completeness to the outer limit of 10 000 au spans 3.5 orders of magnitude. The distribution of projected separations was constructed over six

Table 5. Likelihood of chance proper motion and position matches for low proper motion binaries.

HIP	No. of 5σ synth. μ matches	No. of 10σ synth. μ matches	ρ (asec)	Source density (counts asec $^{-2}$)	No. of Bg. sources (counts)
3937	28	127	1.68	3.15×10^{-3}	2.80×10^{-5}
15220	0	1	4.5	3.21×10^{-5}	2.04×10^{-3}
22738	27	82	7.65	3.02×10^{-6}	5.55×10^{-4}
23452	0	1	0.81	2.15×10^{-6}	4.44×10^{-6}
28368	3	11	163.15	9.54×10^{-6}	7.98×10^{-1}
35191	7	37	0.05	7.28×10^{-6}	5.72×10^{-1}
36626	1	5	0.68	5.28×10^{-6}	7.67×10^{-6}
41824	6	39	11.04	3.42×10^{-6}	1.31×10^{-3}
59406	0	1	84.7	3.24×10^{-6}	7.31×10^{-2}
65026	200	942	0.63	1.56×10^{-6}	1.95×10^{-6}
65714	0	1	8.86	2.87×10^{-6}	7.07×10^{-4}
72944	1	7	4.98	1.59×10^{-6}	1.21×10^{-4}
97292	0	1	5.62	1.06×10^{-4}	1.05×10^{-8}
102141	3	6	2.82	4.21×10^{-6}	1.05×10^{-2}
111802	0	1	25.86	1.50×10^{-6}	3.15×10^{-4}

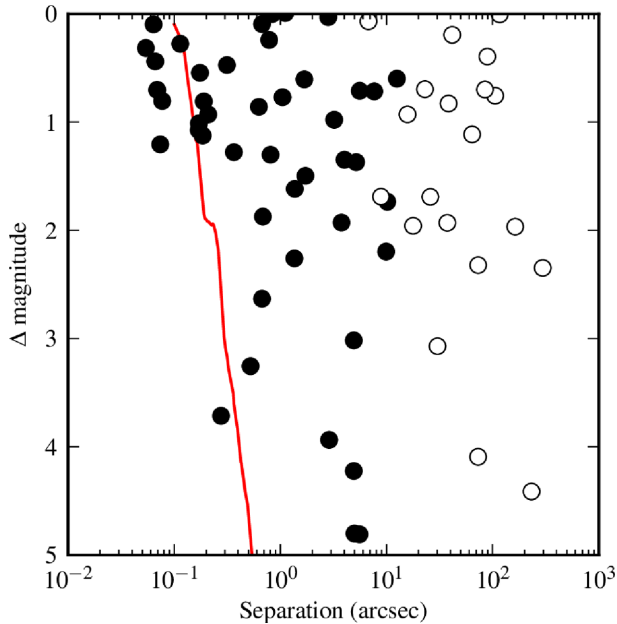


Figure 11. The separations and magnitude differences for the confirmed stellar companions in our survey. Companions shown were detected in either the AO data (in one or more of the JHK_S filters, filled circles), the plate data (only K_S magnitude differences from 2MASS cross-matching shown, open circles), or in a few cases, with both imaging techniques. The red line represents the median 3σ sensitivity of the sample, and continues beyond the canonical substellar limit. The survey is sensitive to companions above, and to the right of, this sensitivity limit.

equally sized bins from $\log(a_{\text{proj}})$ of 0.5 to 4.0, and is shown in Fig. 16. For each bin, the number of targets in the sample that was sensitive to 95 per cent of the bin range is indicated above each bin, and the companion frequency per bin was determined by dividing the number of resolved companions within the bin by the subset of targets complete to 95 per cent of the bin. The error bars were calculated from Poisson statistics.

Over the range of the survey data, the distribution rises monotonically to the smaller separations covered in the 3 to 10 au bin. The best-fitting log-normal distribution is plotted, and due to the unconstrained location of the peak of the distribution, a best-fitting $\mu_{\log(a)} = -0.66$ and $\sigma_{\log(a)} = 1.86$ is found. Fixing the peak to be at

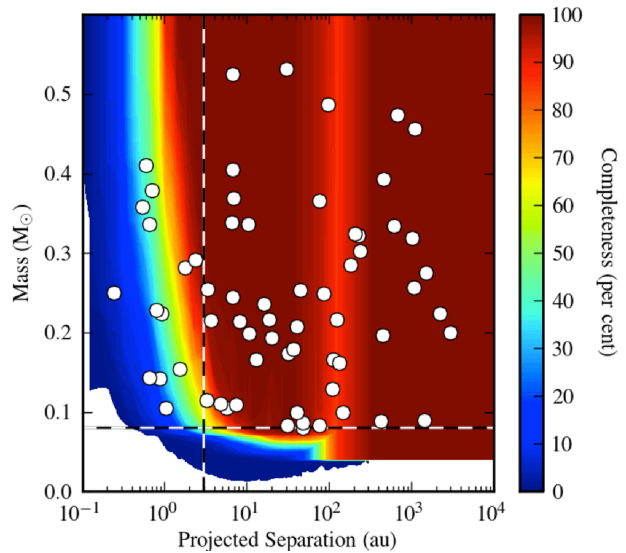


Figure 12. The completeness of the MinMs survey in terms of derived physical parameters. The horizontal black and white dashed line designates the substellar limit of $0.08 M_\odot$, while the vertical dashed line at 3 au indicates the minimum interior separation to which the AO subsample is 85 per cent complete. These lines define the minimum mass and separation thresholds used to assess population statistics for a subsample minimizing detection biases. Stellar companions are overplotted, and span the parameter range of our survey.

the centre of the first bin of the observed distribution [$\mu_{\log(a)} = 0.77$], a significantly narrower distribution is fit ($\sigma_{\log(a)} = 1.34$). Compared to a previous survey of M-stars at a larger range of distances with less sensitivity to wider companions (Janson *et al.* 2012), the peak of the restricted fit to the MinMs distribution is lower, but significantly wider (Fig. 16). Two additional comparison curves are shown for the distributions of companions to higher mass primaries. The solar-type distribution peak occurs at a somewhat wider separation (Raghavan *et al.* 2010) and the fit is consistently higher than the corresponding value of the M-star distribution with the exception of the bin for the smallest separations. The fit to the projected separation distribution of A-star systems (De Rosa *et al.* 2014) is substantially different, with a markedly larger value for the peak and an overall higher normalization. Given the larger distances of the A-star

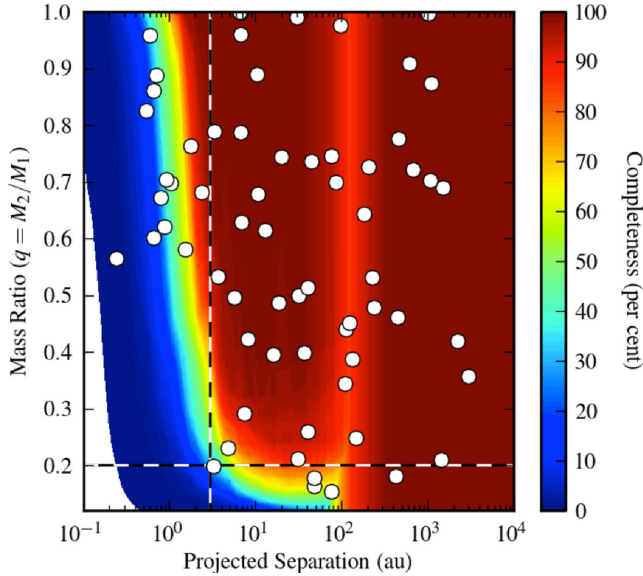


Figure 13. The completeness of the MinMs survey, shown in terms of the mass ratio of the companion to the primary star. The horizontal dashed line at $q = 0.2$ designates the mass ratio limit for uniform completeness, while the vertical dashed line indicates the minimum separation limit of 3 au used to assess population statistics.

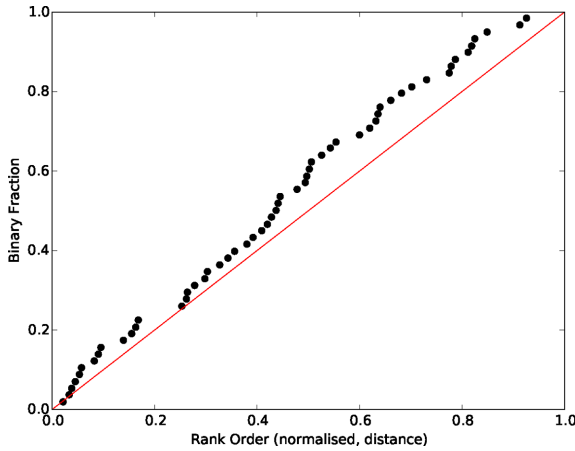


Figure 14. Binary fraction of the stars within our sample at a given distance versus normalized rank-ordered distance of the full sample. The solid red line denotes the expected trend for a random distribution, with integrated area normalized to 0.5 ± 0.03 (errors drawn from Monte Carlo simulations of 10 000 random distributions). The black points show the binary fraction as a function of rank-ordered distance; with an integrated area of 0.54, the binary occurrence is consistent with being drawn from a random distribution, implying an unbiased observation of binaries in the MinMs sample with respect to system distance.

sample ($D \leq 75$ pc), the inner limit for data used to construct the A-star distribution is located at the third bin of the MinMs data ($\log a_{\text{proj}} = 1.6$). Considering the fits to the M-dwarf, solar-type and A-star surveys, the MinMs results provide further evidence to support the trend of a wider typical system separation as a function of host star mass that has been noted in previous studies. The MinMs study refines the population statistics for low-mass stars with the large sample and comprehensive mass and separation sensitivity.

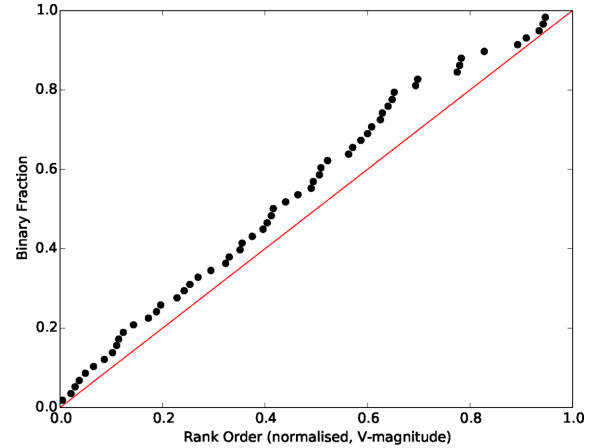


Figure 15. Binary fraction of the stars within our sample with a given V-band magnitude versus normalized rank-ordered magnitude of the full sample. Colours and symbols are as in the preceding figure for distance distribution. The integrated binary distribution with respect to magnitude is also 0.54, and consistent with being drawn randomly, implying an unbiased observation of binaries in the MinMs sample with respect to system brightness.

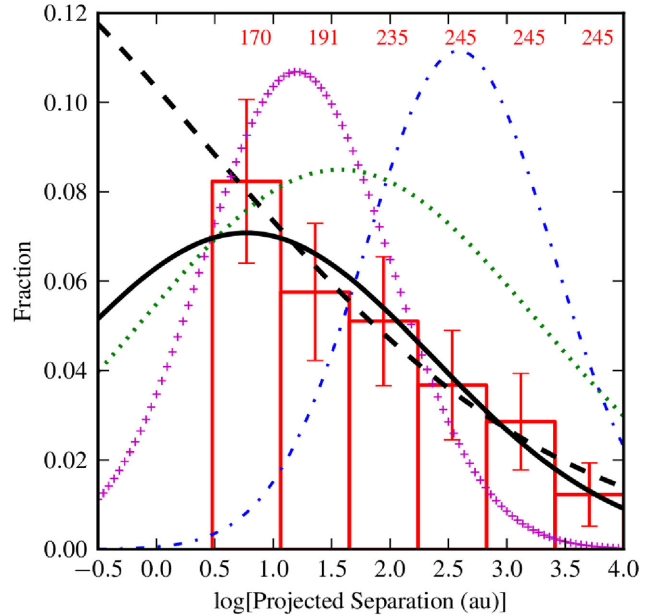


Figure 16. The distribution of projected separations for the companions resolved between 3 and 10 000 au, corrected for incompleteness (red histogram). Assuming a log-normal distribution, a Gaussian was fit to the observed distribution. Allowing all parameters to vary freely, the distribution is best fitted by a Gaussian with a mean of $\mu_{\log(a)} = -0.66$ and width of $\sigma_{\log(a)} = 1.86$ (dashed black curve). A restricted fit was also computed by fixing the mean of the distribution to the centre of the first bin of the distribution ($\mu_{\log(a)} = 0.77$), with a best-fitting Gaussian of width $\sigma_{\log(a)} = 1.34$ (solid black curve). These fits represent the two limiting cases of the true distribution, given the observed distribution within the restricted separation range. For comparison, the distribution of companion separations for A-star primaries (blue dot-dashed curve, De Rosa et al. 2014), solar-type primaries (green dotted curve, Raghavan et al. 2010), and for M-dwarf primaries in a previous lucky-imaging survey (magenta crosses, Janson et al. 2012).

5.4 Mass ratio distribution

Based on the survey completeness shown in Fig. 13, the systems included in the mass ratio distribution have a mass ratio of $q \geq 0.2$. The shape of the observed mass ratio distribution is consistent with a flat distribution, as shown in Fig. 17. Because the target masses are close to the stellar limit, all targets are not sensitive to the full range of mass ratios ($q \geq 0.2$). The median mass of a star in the sample is $\sim 0.44 M_{\odot}$ and the mass ratio limit for the median star corresponds to a secondary mass limit of $0.09 M_{\odot}$. For the lowest-mass stars in the sample, the bottom of the main sequence occurs at a mass ratio greater than $q > 0.2$. As the lowest-mass primaries in our sample have masses in the 0.12 – $0.18 M_{\odot}$ range, corresponding to a companion at the stellar/substellar boundary with $q \sim 0.6$, the two lowest mass ratio bins are affected by this potential bias.

The mass ratio values were sorted by the separation of the pair and split into two sets by a range of dividing separations, and the inner and outer distributions were compared to each other with a Kolmogorov–Smirnov (KS) test. The inner and outer distributions were not found to be significantly different, regardless of the dividing separation used. This result is different from what was found for both G-star (Raghavan *et al.* 2010) and A-star binaries (De Rosa *et al.* 2014). Since there was no difference in the mass ratio distributions, the full set of companions was used to investigate the shape of the true underlying distribution. In order to estimate the expected shape of the mass ratio distribution, taking into account the distribution of primary masses, we performed a series of Monte Carlo simulations to construct comparison mass ratio distributions from pairing the MinMs primaries with secondaries of different companion mass ratio functions (Fig. 17).

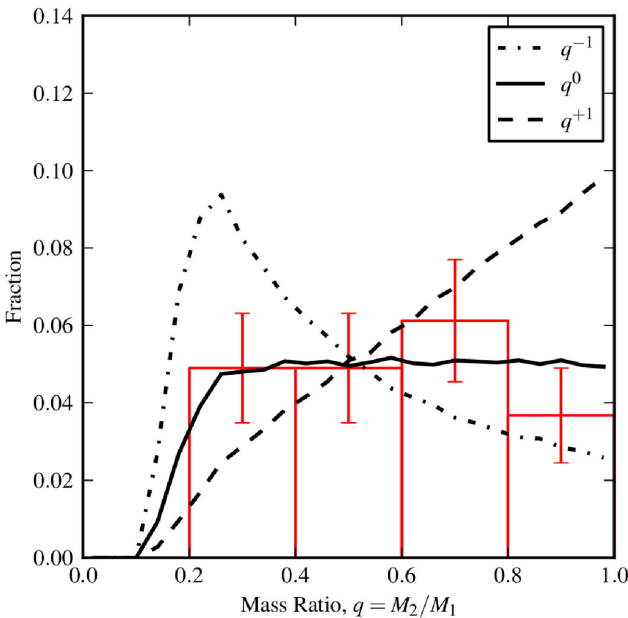


Figure 17. The distribution of companion mass ratios for the companions resolved in the MinMs study. Only those companions with projected separations between 30 and 10 000 au and mass ratios of $q \geq 0.2$ are included to minimize observational biases. The predicted shape of the mass ratio distribution for companions drawn from a distribution rising to more equal-mass companions [$f(q) \propto q^1$, dashed curve], a flat distribution [$f(q) \propto q^0$, solid curve], and a falling distribution [$f(q) \propto q^{-1}$, dot-dashed curve] are plotted for reference. The observed mass ratio distribution is most consistent with the flat distribution.

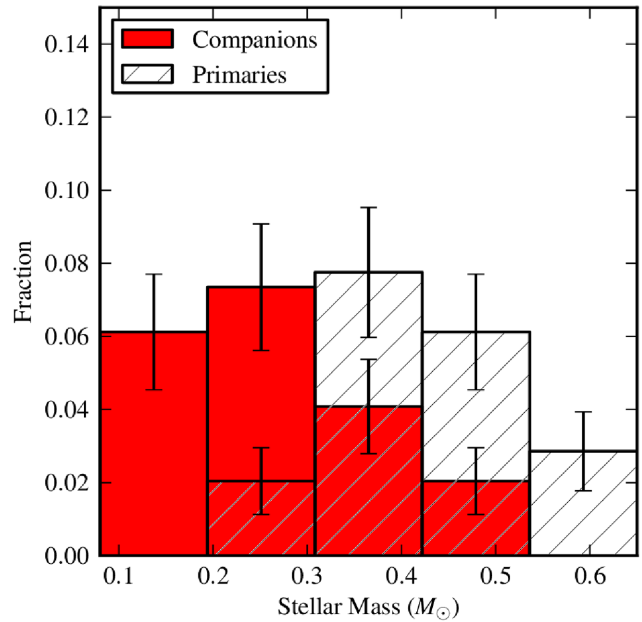


Figure 18. The distribution of primary masses and companion masses for all stellar companions and hosts found within the MinMs study, shown in fractions of the total sample. A KS test performed on the single star masses against the masses of primaries in binaries showed no preference towards stellar mass correlating with presence of companions over the K7–M6 spectral type range of our sample.

We have assumed that the full mass range of the MinMs primaries can be described as a simple population with a single underlying mass ratio distribution. The pairing simulations were based on a population of 1×10^5 primary stars with a distribution of masses matching the primaries in the MinMs survey. For each primary, a companion mass was drawn randomly from rising, falling, or uniform mass ratio distributions over the full stellar companion mass range of $0.08 M_{\odot}$ to the given primary mass, producing 1×10^5 companions. We then divided the masses of the secondaries by the masses of the primaries to obtain the corresponding mass ratios. From this analysis, only those stars with $M_{\odot} < 0.4$ were biased against detecting mass ratios of $q < 0.2$ (making up 35 per cent of the sample) and given that the sample stars fall off quickly towards lower-mass primaries, only 10 per cent of primaries $< 0.3 M_{\odot}$ were similarly biased, resulting in a bias in half of the $q = 0.2$ – 0.4 bin. In this way, the rising, falling and uniform distributions are compared with similar completeness to the mass ratio distribution of the observed companions. This is similar to previous analyses for higher-mass primaries, and statistical analyses of companion mass ratio distributions (Reggiani & Meyer 2011, 2013). In light of our implicit assumption that the q -distribution is the same for the full range of MinMs primaries, the observed mass ratio distribution is thus consistent with companions drawn from a distribution flat in mass ratio ($f(q) \propto q^0$).

5.5 Companion and total system mass distributions

Given the high level of completeness to the bottom of the main sequence, the distributions of primary and companion mass were constructed for all pairs with > 3 au projected separation. Unlike the flat mass ratio distribution, the companion mass distribution shown in Fig. 18 rises continuously with decreasing mass. Similarly, the total system mass distribution in Fig. 19 rises to smaller masses.

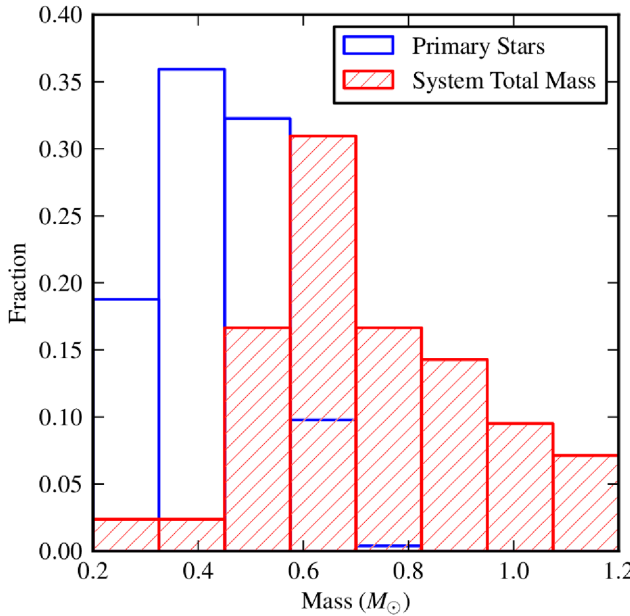


Figure 19. The distribution of total system mass, calculated as the sum of all components within a given multiple system, including all companions with separations of $a_{\text{proj}} \geq 3$ au and $q \geq 0.2$, normalized by the number of such companions (red hatched histogram). Plotted for reference is the distribution of primary masses given in Fig. 4, normalized by the overall sample size (blue histogram).

For comparison, a KS test was performed to compare the mass distribution of single stars and that of primaries in binary systems; with a p -value of 0.34, no intrinsic difference was found between the two populations, indicating no preference for massive primaries having more companions (or vice versa). For triple and quadruple systems, all companions and the primary are summed to determine the system mass included in Fig. 18. For comparison with the total system distribution, the target star mass distribution is also plotted in Fig. 19.

5.6 Frequency of companions

There are two quantities that define the multiplicity of the sample. The multiplicity fraction (MF) quantifies the number of multiple systems within the sample:

$$\text{MF} = \frac{b + t + q + \dots}{s + b + t + q + \dots}, \quad (3)$$

where s is the number of singles, b the number of binaries, t the number of triples, q the number of quadruples, and so forth (e.g. Reipurth & Zinnecker 1993; Goodwin, Whitworth & Ward-Thompson 2004). The companion star fraction (CSF) quantifies the total number of companions within the sample as the following:

$$\text{CSF} = \frac{b + 2t + 3q + \dots}{s + b + t + q + \dots}, \quad (4)$$

(Patience et al. 2002). As described in Section 5.1, AO data exist for a subsample of 196 stars within the 245-star MinMs sample. Therefore, the MF can be calculated for separate subsamples, accounting for selection effects over different ranges of projected separation. Of the AO data, which form a subsample searching projected separations in the 1–100 au range, we find 41 binaries of the 196 stars with AO imaging, corresponding to a MF of 21 ± 3 per cent. For

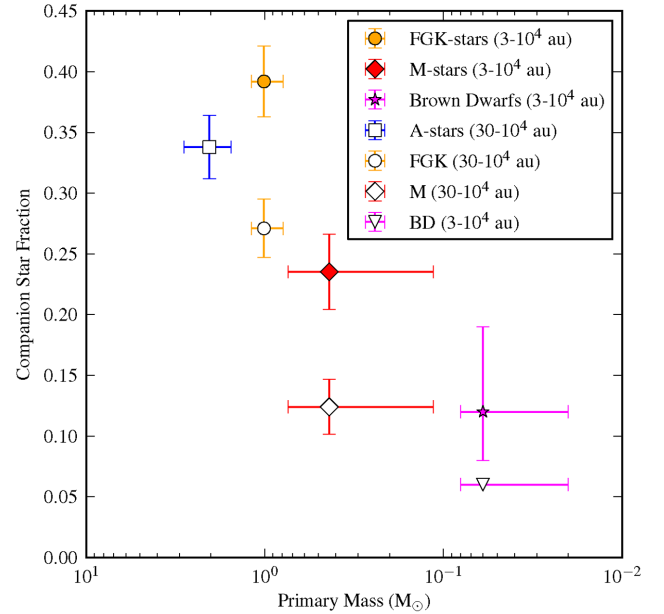


Figure 20. The CSFs measured over the full 3–10 000 au (filled symbol) and restricted 30–10 000 au (open symbol) separation ranges. Comparison values for both ranges, from left to right, are shown for solar-type stars (yellow circles, Raghavan et al. 2010), and M-dwarfs (red diamonds, this study). Over the 3–10 000 au range, a measured value exists for brown dwarf primaries (pink star, Burgasser et al. 2006). Over the restricted 30–10 000 au range, additional comparison values are available for field A-type stars (blue square, De Rosa et al. 2014), as well as an upper limit to the $\text{CSF}_{30 - 10\,000\,\text{au}}$ for brown dwarf primaries (pink downward triangle, Allen et al. 2007), demonstrating the decreasing trend of multiplicity with later spectral type.

the plate data, we find 17 wide binaries covering the 100–10 000 au range within the full 245 star sample with plate imaging, corresponding to a MF for the wide subsample of 7 ± 2 per cent. This is consistent with the tighter semi-major axis distribution and lower multiplicity seen in comparison to higher-mass primaries.

The CSF over 3–10 000 au is calculated by summing the fraction in each separation bin of Fig. 16, since each bin is already corrected for incompleteness. The resulting $\text{CSF}_{3-10\,000\,\text{au}}$ value is 23.5 ± 3.2 per cent, as shown in Fig. 20. For closer separations, the survey is not fully sensitive to the bottom of the main sequence, but a lower limit on the total CSF can be estimated by combining the bound companions resolved within this study with those reported within the WDS catalogue and the Ninth catalogue of Spectroscopic Binary Orbits (SB9; Pourbaix et al. 2004). The resulting $\text{CSF}_{\text{total}}$ is $34.7^{+2.9}_{-3.2}$ per cent. (Similarly, the lower limit on the total multiplicity of the sample was estimated as $\text{MF}_{\text{total}} = 28.6^{+2.7}_{-3.1}$ per cent.)

To place the MinMs results in a broader context, the CSF is compared with samples with different primary star masses. Two separation ranges are considered: the full 3–10 000 au range and the more restrictive 30–10 000 au range. The 3–10 000 au range requires samples of nearby field objects to reach the smaller projected separations, so the MinMs value is compared with field solar-type stars (Raghavan et al. 2010) and field brown dwarfs (Burgasser et al. 2006). As shown in Fig. 20, the CSF calculated over both separation ranges shows a decline with primary mass. The solar-type star study was sensitive to the bottom of the main sequence as is the case for the MinMs survey, while the surveys of brown dwarfs were typically sensitive to $q \gtrsim 0.5$. Over the restricted 30–10 000 au range, for which a $\text{CSF}_{30-10\,000\,\text{au}} = 12.4 \pm 2.3$ per cent was measured for

the M-dwarf primaries within this study, it is possible to include the results from the more massive A-stars (De Rosa *et al.* 2014). Due to the paucity of wide companions to brown dwarfs, there is only an upper limit on the brown dwarf CSF over this separation range (Allen *et al.* 2007).

5.7 Higher order multiple systems

Since the MinMs companions include a large range of separations from a minimum of 0.2 au to a maximum of 2,952 au, and ~ 200 stars have both AO and wide field imaging, it is possible to detect higher order multiple systems within the survey. A total of three triple and two quadruple systems were identified. All the triple systems are in hierarchical arrangements and the ratio of inner to outer projected separations ranges from 347:1 to 27:1. The threshold for stability of multiple systems is considered to be a separation ratio for the outer to inner pair of 5:1 (Eggleton 2006), suggesting that all the triple systems are likely stable. For the two quadruples, one system consists of two widely separated close pairs, while the other system is composed of a close pair and two wider and lower mass stars. For a full accounting of the frequency of higher order multiples, radial velocity measurements of the sample with AO and wide field imaging are required.

To determine whether any spectroscopic systems were previously known within the sample, we cross-referenced the SB9 catalogue and the 70 star M-dwarf spectroscopic survey by Marcy & Benitz (1989, hereafter MB89) against our sample. Among the 50 MinMs stars within the MB89 study, only two spectroscopic binaries are known. From the cross-reference with SB9, an additional 10 spectroscopic binaries were identified within our sample from the following surveys, listed in Table 6: Nidever *et al.* 2002 (N02), Evans 1959 (E59), Tomkin & Pettersen 1986 (TP86), Tokovinin 1997 (T97), Mazeh *et al.* 2001 (M01), and Herbig & Moorhead 1965 (HM65). Of these spectroscopic systems, one was resolved in archival AO imaging (HIP 9724). As the completeness of the SB9 catalogue is unknown since non-detections are not reported, we do not include these binaries in our analysis. The incompleteness of the spectroscopic results underscores the need for a comprehensive spectroscopic companion survey of nearby M-dwarfs, such as the CARMENES survey (Quirrenbach *et al.* 2010). By building upon the current results, the MinMs sample represents an ideal target set for developing a comprehensive understanding of the frequency and properties of higher-order multiple systems with low-mass primaries.

Table 6. Summary of known spectroscopic binaries in the MinMs sample.

HIP	Reference	SB type	Period (d)	AO resolved?
9724	N02	1	6818	Yes
11964	E59	1	1.962	No
25953	MB89	2	–	No
34603	TP86	1	10.428	No
38082	MB89	2	–	No
65011	T97	1	200.26	No
76901	N02	1	62.628	No
80346	N02	1	1366.1	No
82809	M01	1	2.9655	No
82817	M01	1	2.9655	No
111802	HM65	1	4.0832	No

6 SUMMARY AND CONCLUSIONS

With a combination of multi-epoch AO and wide-field imaging, we have conducted a companion search programme targeting 245 late K- and early M-dwarfs which are within 15 pc with *Hipparcos* parallax uncertainties of < 10 per cent, $M_V > 8$, and which are not companions to earlier spectral-type primaries. Companions with projected separations as small as 0.2 au were resolved, and beginning at a separation of 3 au and continuing to 10 000 au, the observations were sensitive to the companions down to the stellar/substellar limit. Within this complete range, a total of 65 comoving companions were detected, 47 with AO observations and 18 from wide-field imaging data, of which four are newly resolved within this study.

Over the complete 3–10 000 au separation range, the CSF is 23.5 ± 3.2 per cent. With the large sample size, the uncertainties are reduced by a factor of ~ 2 relative to previous studies, which makes it possible to determine that the M-dwarf CSF is distinctly lower than the solar-type value (Raghavan *et al.* 2010) and higher than the corresponding brown dwarf fraction (Burgasser *et al.* 2006). By considering the separation range of 30–10 000 au to enable a comparison with the more distant and more massive A-stars (De Rosa *et al.* 2014), a $\text{CSF}_{30-10\,000\,\text{au}} = 12.4 \pm 2.3$ was measured, and a systematic decline in CSF as a function of primary mass is observed.

Dividing the observed range of companion separations into six bins, the separation distribution is seen to rise continuously towards the smallest separations to which the survey is sensitive. When compared to the results of a previous lucky imaging survey of M-dwarfs (Janson *et al.* 2012), the MinMs distribution appears to have a wider spread, likely due to the enhanced coverage that enabled a direct measurement of the widest systems. The mass ratio distribution is flat across the $q = 0.2\text{--}1.0$ range, similar to that observed for companions to solar-type stars (Raghavan *et al.* 2010), but different from the rise towards lower mass ratios seen for higher-mass stars (De Rosa *et al.* 2014).

The MinMs study can serve as a benchmark data set for comparisons with the companion star properties of more distant populations of young low-mass stars. Given the existing large coverage, the MinMs sample is also an ideal set to pursue radial velocity searches for the closest companions to complete the separation distribution, and to provide the first complete accounting of high order multiplicity of M-dwarfs.

ACKNOWLEDGEMENTS

The authors wish to thank the anonymous referee for providing a thorough review and helpful comments which improved this manuscript. KWD is supported by the National Science Foundation Graduate Research Fellowship under Grant No. DGE-1311230. RJDR acknowledges support from Science and Technology Facilities Council grants ST/H002707/1 and ST/K005588/1. RJP acknowledges support from the Royal Astronomical Society in the form of a research fellowship. We are grateful to the MMT Observatory staff for their excellent support of these observations. We also thank B. Svoboda for valuable programming discussions. This research has made use of the SIMBAD data base, operated at CDS, Strasbourg, France. This research makes use of data products from the 2MASS, which is a joint project of the University of Massachusetts and the Infrared Processing and Analysis Center/California Institute of Technology, funded by the National Aeronautics and Space Administration and the National Science Foundation. This research has made use of the WDS catalogue maintained at the US Naval Observatory. This research used the facilities of the Canadian Astronomy Data Centre operated by the National

Research Council of Canada with the support of the Canadian Space Agency. Results are based on data obtained from the ESO Science Archive Facility. Based in part on data collected at Subaru Telescope and obtained from the SMOKA, which is operated by the Astronomy Data Center, National Astronomical Observatory of Japan. This research has made use of data obtained from the SuperCOSMOS Science Archive, prepared and hosted by the Wide Field Astronomy Unit, Institute for Astronomy, University of Edinburgh, which is funded by the UK Science and Technology Facilities Council.

REFERENCES

- Allen P. R., Koerner D. W., McElwain M. W., Cruz K. L., Reid I. N., 2007, AJ, 133, 971
- Andrews S. M., Wilner D. J., Hughes A. M., Qi C., Dullemond C. P., 2009, ApJ, 700, 1502
- Artymowicz P., Lubow S. H., 1994, ApJ, 421, 651
- Baba et al., 2002, ASPC, 281, 298
- Baraffe I., Chabrier G., Allard F., Hauschildt P. H., 1998, A&A, 337, 403
- Bastian N., Covey K. R., Meyer M. R., 2010, ARA&A, 48, 339
- Bergfors C. et al., 2010, A&A, 520, A54
- Bertin E., Arnouts S., 1996, A&AS, 117, 393
- Beuzit J.-L. et al., 2004, A&A, 425, 997
- Browning M. K., Basri G., Marcy G. W., West A. A., Zhang J., 2010, AJ, 139, 504
- Burgasser A. J., Kirkpatrick J. D., Cruz K. L., Reid I. N., Leggett S. K., Liebert J., Burrows A., Brown M. E., 2006, ApJS, 166, 585
- De Rosa R. J. et al., 2011, MNRAS, 415, 854
- De Rosa R. J. et al., 2014, MNRAS, 437, 1216
- Doyon R., Nadeau D., Vallee P., Starr B. M., Cuillandre J. C., Beuzit J.-L., Beigbeder F., Brau-Nogue S., 1998, in Fowler A. M., ed., SPIE Conf. Ser. Vol. 3354, Society of Photo-Optical Instrumentation Engineers (SPIE) Conference Series, p. 760
- Eggleton P., 2006, Evolutionary Processes in Binary and Multiple Stars. Cambridge Univ. Press, Cambridge
- ESA, 1997, EAS Publ. Ser. Vol. 1200, The Hipparcos and Tycho catalogues. Astrometric and photometric star catalogues derived from the ESA Hipparcos Space Astrometry Mission, ESA Publ., Noordwijk, Netherlands
- Evans D. S., 1959, MNRAS, 119, 526
- Fischer D. A., Marcy G. W., 1992, ApJ, 396, 178
- Gaidos E., Mann A. W., 2014, ApJ, 791, 54
- Gini C., 1955, Memorie di metodologica statistica, 1, 156
- Goodwin S. P., 2010, R. Soc. Lond. Philosophical Trans. Ser. A, 368, 851
- Goodwin S. P., Whitworth A. P., Ward-Thompson D., 2004, A&A, 423, 169
- Gray R. O., Corbally C. J., Garrison R. F., McFadden M. T., Bubar E. J., McGahee C. E., O'Donoghue A. A., Knox E. R., 2006, AJ, 132, 161
- Hambly N. C. et al., 2001, MNRAS, 326, 1279
- Hawley S. L., Gizis J. E., Reid I. N., 1996, AJ, 112, 2799
- Heintz W. D., 1986, A&AS, 65, 411
- Henry T. J., Jao W.-C., Subasavage J. P., Beaulieu T. D., Ianna P. A., Costa E., Méndez R. A., 2006, AJ, 132, 2360
- Herbig G. H., Moorhead J. M., 1965, ApJ, 141, 649
- Hodapp K. W. et al., 2008, in SPIE Conf. Ser. Vol. 7014, Society of Photo-Optical Instrumentation Engineers (SPIE) Conference Series
- Houk N., Cowley A. P., 1975, University of Michigan Catalogue of Two-dimensional Spectral Types for the HD stars. Volume I. Declinations-90 to -53.
- Janson M. et al., 2012, ApJ, 754, 44
- Kenyon S. J., Hartmann L., 1995, ApJS, 101, 117
- King R. R., Goodwin S. P., Parker R. J., Patience J., 2012a, MNRAS, 427, 2636
- King R. R., Parker R. J., Patience J., Goodwin S. P., 2012b, MNRAS, 421, 2025
- Kobayashi N. et al., 2000, in Iye M., Moorwood A. F., eds, SPIE Conf. Ser. Vol. 4008, Optical and IR Telescope Instrumentation and Detectors, p. 1056
- Koen C., Kilkenny D., van Wyk F., Marang F., 2010, MNRAS, 403, 1949
- Kozai Y., 1962, AJ, 67, 591
- Lenzen R. et al., 2003, in Iye M., Moorwood A. F. M., eds, SPIE Conf. Ser. Vol. 4841, Society of Photo-Optical Instrumentation Engineers (SPIE) Conference Series, p. 944
- Lépine S., Gaidos E., 2011, AJ, 142, 138
- Lidov M. L., 1962, Planet. Space Sci., 9, 719
- Luhman K. L., Stauffer J. R., Muench A. A., Rieke G. H., Lada E. A., Bouvier J., Lada C. J., 2003, ApJ, 593, 1093
- Luhman K. L., Allen P. R., Espaillat C., Hartmann L., Calvet N., 2010, ApJS, 186, 111
- McCarthy D. W., Burge J. H., Angel J. R. P., Ge J., Sarlot R. J., Fitz-Patrick B. C., Hinz J. L., 1998, in Fowler A. M., ed., SPIE Conf. Ser. Vol. 3354, Infrared Astronomical Instrumentation. p. 750
- Marcy G. W., Benitz K. J., 1989, ApJ, 344, 441 (MB89)
- Mason B. D., Wycoff G. L., Hartkopf W. I., Douglass G. G., Worley C. E., 2001, AJ, 122, 3466
- Mazeh T. et al., 2001, MNRAS, 325, 343
- McCook G. P., Sion E. M., 1999, ApJS, 121, 1
- Metchev S. A., Hillenbrand L. A., 2009, ApJS, 181, 62
- Murakawa K. et al., 2003, in Iye M., Moorwood A. F. M., eds, SPIE Conf. Ser. Vol. 4841, Instrument Design and Performance for Optical/Infrared Ground-based Telescopes, p. 881
- Murakawa K. et al., 2004, PASJ, 56, 509
- Neves V., Bonfils X., Santos N. C., Delfosse X., Forveille T., Allard F., Udry S., 2014, A&A, 568, A121
- Newton E. R., Charbonneau D., Irwin J., Berta-Thompson Z. K., Rojas-Ayala B., Covey K., Lloyd J. P., 2014, AJ, 147, 20
- Nidever D. L., Marcy G. W., Butler R. P., Fischer D. A., Vogt S. S., 2002, ApJS, 141, 503
- Parker R. J., Goodwin S. P., 2009, MNRAS, 397, 1041
- Parker R. J., Meyer M. R., 2014, MNRAS, 442, 3722
- Parker R. J., Quanz S. P., 2013, MNRAS, 436, 650
- Patience J. et al., 2002, ApJ, 581, 654
- Perryman M. A. C. et al., 1997, A&A, 323, L49
- Pourbaix D. et al., 2004, A&A, 424, 727
- Poveda A., Allen C., Costero R., Echevarría J., Hernández-Alcántara A., 2009, ApJ, 706, 343
- Quirrenbach A. et al., 2010, in SPIE Conf. Ser. Vol. 7735, Society of Photo-Optical Instrumentation Engineers (SPIE) Conference Series
- Raghavan D. et al., 2010, ApJS, 190, 1
- Reggiani M. M., Meyer M. R., 2011, ApJ, 738, 60
- Reggiani M., Meyer M. R., 2013, A&A, 553, A124
- Reid I. N., Gizis J. E., 1997, AJ, 113, 2246
- Reid I. N., Hawley S. L., Gizis J. E., 1995, AJ, 110, 1838
- Reipurth B., Zinnecker H., 1993, A&A, 278, 81
- Robin A. C., Reylé C., Derrière S., Picaud S., 2003, A&A, 409, 523
- Roeser S., Demleitner M., Schilbach E., 2010, AJ, 139, 2440
- Rojas-Ayala B., Covey K. R., Muirhead P. S., Lloyd J. P., 2012, ApJ, 748, 93
- Rousset G. et al., 2003, in Wizinowich P. L., Bonaccini D., eds, SPIE Conf. Ser. Vol. 4839, Society of Photo-Optical Instrumentation Engineers (SPIE) Conference Series, p. 140
- Silvestri N. M., Oswalt T. D., Wood M. A., Smith J. A., Reid I. N., Sion E. M., 2001, AJ, 121, 503
- Skrutskie M. F. et al., 2006, AJ, 131, 1163
- Tokovinin A. A., 1997, A&AS, 121, 71
- Tokovinin A., 2008, MNRAS, 389, 925
- Tokunaga A. T. et al., 1998, in Fowler A. M., ed., SPIE Conf. Ser. Vol. 3354, Infrared Astronomical Instrumentation. p. 512
- Tomkin J., Pettersen B. R., 1986, AJ, 92, 1424
- Torres C. A. O., Quast G. R., da Silva L., de La Reza R., Melo C. H. F., Sterzik M., 2006, A&A, 460, 695
- van Leeuwen F., 2007, A&A, 474, 653
- Wenger et al., 2000, A&AS, 143, 9
- Worley C. E., 1962, AJ, 67, 396
- Wu Y., Murray N., 2003, ApJ, 589, 605

APPENDIX A

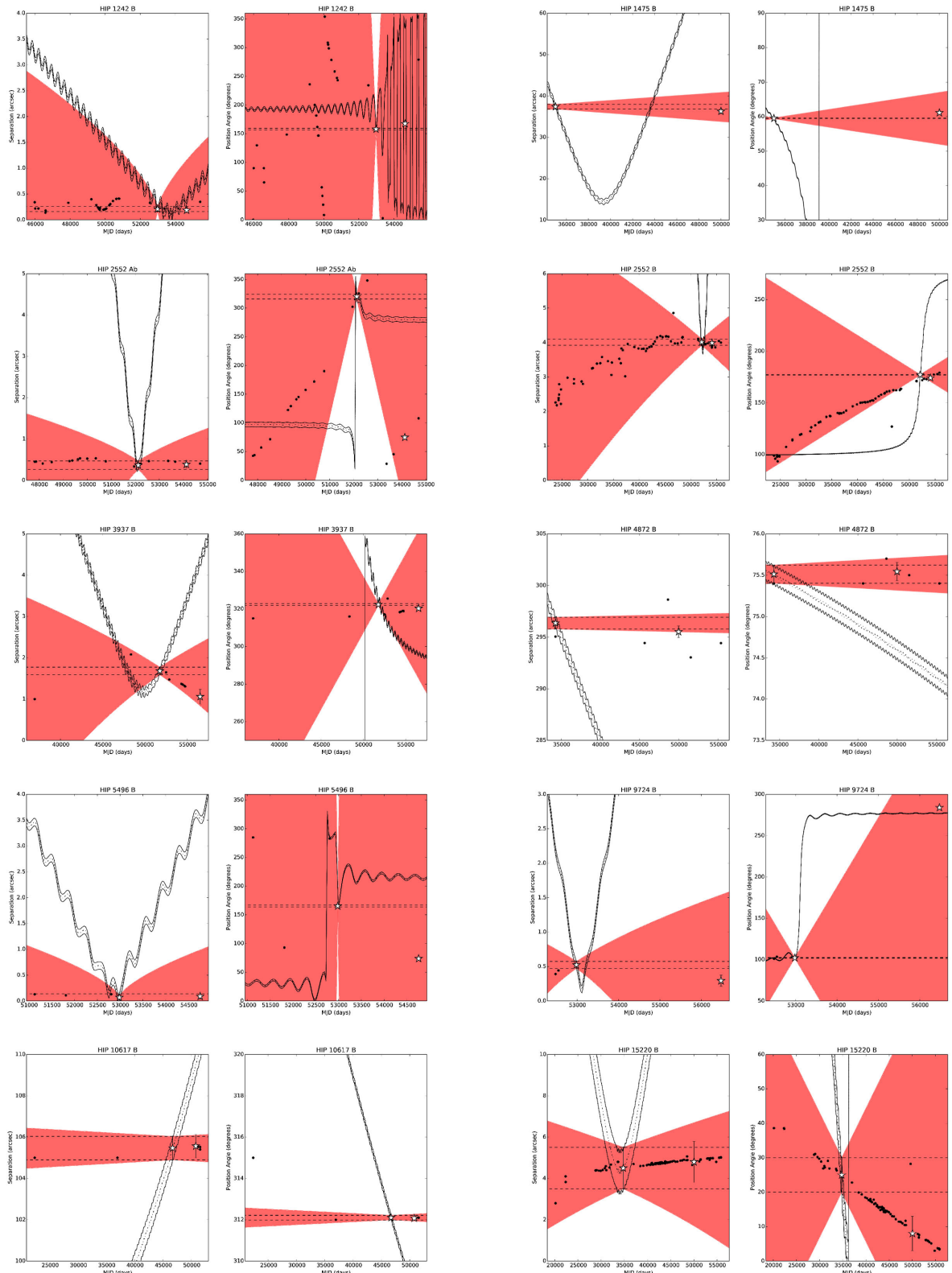


Figure A1. Sample proper motion diagrams of the bound companions identified within this study. Symbols, curves, and shading are as in Fig. 6. The full set of proper motion diagrams for each of the detected companion candidates in this study is available in the electronic edition of the journal.

Table A1. Companion detection limits.[†]

HIP	AO Δm (mag) at $\rho = (\text{arcsec})$									ρ sensitive to full MS		
	0.05	0.15	0.25	0.50	1.00	1.50	2.00	5.00	10.00	$\rho_{\text{AO, max}}$ (arcsec)	$\rho_{\text{Plate, min}}$ (arcsec)	$\rho_{\text{Plate, max}}$ (arcmin)
HIP 428	...	0.64	1.87	4.33	6.67	8.08	8.71	9.18	9.17	34.00	5.64	14.81
HIP 439	0.02	3.87	5.04	6.23	6.41	6.39	6.40	6.36	4.11	14.00	21.58	38.40
HIP 1242	0.01	2.70	2.09	6.34	7.04	7.04	7.07	7.01	4.48	13.00	2.50	33.42
HIP 1475	...	0.89	1.91	4.37	6.16	7.88	8.20	8.51	8.51	35.00	12.49	46.46
HIP 2552	...	0.63	1.49	2.36	5.14	6.76	7.75	6.47	7.90	39.00	5.37	16.56
HIP 3937	...	0.61	0.87	1.89	2.55	1.35	1.64	7.50	8.79	36.00	6.30	14.07
HIP 4569	5.40	13.49
HIP 4856	...	0.69	1.94	4.28	6.90	8.02	8.63	9.52	9.34	38.00	7.93	20.24
HIP 4872	...	1.10	2.00	4.46	6.58	8.29	8.65	9.02	8.94	35.00	8.46	16.73
HIP 5496	0.08	1.09	3.48	4.93	6.82	7.25	7.29	7.22	6.71	13.00	8.09	20.34

[†]Table A1 is published in its entirety in the electronic edition of the journal. A portion is shown here for guidance regarding its form and content.

SUPPORTING INFORMATION

Additional Supporting Information may be found in the online version of this article:

Table 1. The 245 K7-M6 dwarf sample within 15 pc.

Table 2. High-resolution imaging data.

Table A1. Companion detection limits.

Figure A1. Sample proper motion diagrams of the bound companions identified within this study.

(<http://mnras.oxfordjournals.org/lookup/suppl/doi:10.1093/mnras/stv384/-DC1>).

Please note: Oxford University Press is not responsible for the content or functionality of any supporting materials supplied by the authors. Any queries (other than missing material) should be directed to the corresponding author for the article.

This paper has been typeset from a \TeX / \LaTeX file prepared by the author.